

https://dspace.org/

Sliding wear resistance of the CobaltBased Coatings ULTIMETTM and STELLITETM 6 with ruthenium additions

Silas Hango; Lesley Cornish; Lesley Chown; Johannes Van der Merwe; F.P.L Kavishe

PERGAMON-ELSEVIER SCIENCE LTD
https://hdl.handle.net/10539/42871
WOS

Downloaded from a DSpace repository. https://dspace.org/

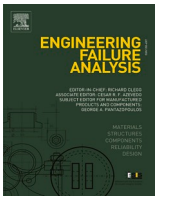
Engineering Failure Analysis 155 (2024) 107717



Contents lists available at ScienceDirect

Engineering Failure Analysis

journal homepage: www.elsevier.com/locate/engfailanal





Sliding wear resistance of the Cobalt-Based Coatings, ULTIMET^{TM} and STELLITE^{TM} 6 with ruthenium additions

Silas I. Hango [a,b,*], Lesley A. Cornish [a], Lesley H. Chown [a], Josias W. van der Merwe [a], Frank P.L. Kavishe [b,1]

[a] School of Chemical and Metallurgical Engineering and DSI-NRF Centre of Excellence in Strong Materials and African Materials Science and Engineering Network (AMSEN), University of the Witwatersrand, Private Bag 3, WITS, 2050, Johannesburg, South Africa
[b] Department of Mechanical and Metallurgical Engineering, University of Namibia, P.O. Box 3624, Ongwediva, Namibia

ARTICLE INFO

Keywords:
Materials Engineering
Cobalt-based coatings and alloys
coatings with Ru additions
Hardness
Sliding wear

ABSTRACT

Two different cobalt-based bulk alloys, ULTIMET^{TM} and STELLITE^{TM} 6B, their high velocity oxygen fuel (HVOF) spayed coatings with minor additions of ruthenium and mild steel substrate were subjected to ball-on-disc sliding wear tests at 5 N and 10 N and hardness tests at 3 kg. These materials were targeted as replacements or protective coatings on mild steel for better wear resistance. Their microstructures comprised γ-austenite and Cr_3C_2 phases, and coefficients of friction fluctuated slightly. The coatings had good wear resistance ($0.2 \pm 0.0x10^{-5}$–$5.6 \pm 0.2x10^{-5}$ $mm^3{\cdot}N^{-1}{\cdot}m^{-1}$) and higher hardnesses (386 ± 21–547 ± 39 HV_3) than the alloys (304 ± 22–368 ± 13 HV_3) and mild steel (180 ± 14 HV_3). After wear, bulk and coated samples exhibited tearing, slip bands, grooves and debris. The best alloy was STELLITE^{TM} 6 coating with 0.6 wt% Ru addition which had low wear rates both at 5 N ($0.2 \pm 0.0x10^{-5}$ $mm^3{\cdot}N^{-1}{\cdot}m^{-1}$) and 10 N loading ($0.5 \pm 0.0x10^{-5}$ $mm^3{\cdot}N^{-1}{\cdot}m^{-1}$), and was the hardest ($547 \pm 39$ HV_3).

1. Introduction

Tribology is the science and technology of interacting surfaces in relative motion, which encompasses the study and applications of not only friction but also wear and lubrication [1,2]. Friction is due to the loss of energy, wear results in loss of surface material, while lubrication leads to loss of load between two surfaces moving relative to each [2]. The main common wear mechanisms are adhesion, abrasion, fatigue and corrosive wear, resulting in grooves, debris, delamination, tearing and slip [2].

Cobalt-based alloys and coatings have been widely used in many industrial fields, including medical, aerospace and automobile applications, due to their outstanding mechanical, wear and corrosion resistance properties [3–8]. Due to these properties, cobalt-based alloys and coatings were studied to replace or protect mild steel pump components such as casings, sleeves and valves, experiencing wear [9]. The alloys are mainly Co, with Cr to strengthen the Co matrix and form chromium carbide, as well as a protective passive film of chromium oxide, and W is sometimes added to improve hardness [6,10]. Several cobalt-based alloys such as as-cast ULTIMET^{TM} (Co-Cr-Ni-Mo-Fe-W-Mn-Si-N-C) and wrought STELLITE^{TM} 6B (Co-Cr-W-Fe-Ni-Mo-Mn-Si-C) are used as wear resistant coatings on steels [11–13].

Cobalt-based materials are made for dental and orthopaedic implants such as hips, pins, plates, and replacement bone, due to their

* Corresponding author.
E-mail address: shango@unam.na (S.I. Hango).
[1] Deceased author.

https://doi.org/10.1016/j.engfailanal.2023.107717
Received 14 August 2023; Received in revised form 22 September 2023; Accepted 9 October 2023
Available online 18 October 2023
1350-6307/© 2023 Elsevier Ltd. All rights reserved.

excellent tribological resistant properties [5,14,15]. Additionally, they are used in many applications as cutting tools and hard-facing castings in many industries such as power generation, steel manufacturing, chemical processing, oil and gas and marine environments [16,17].

Cobalt-based alloys such as Co-Cr-Mo and Co-Cr-W possess good wear resistance due to their high carbon contents, similar to WC-Co based alloys [18]. The wear resistance of cobalt-based alloys is better than stainless steels and titanium-based alloys [19]. These wear-resistant cobalt-based alloys are usually strengthened with solutes such as Mo and W or by precipitation of Cr- or W- based carbides, such as Cr_7C_3, $Cr_{23}C_6$, WC, W_2C, etc., dispersed in the fcc cobalt-chromium solid solution matrix [15,20,21], e.g. Co-Cr-W/Mo. The carbides provide resistance to low-stress (or two-body) abrasion, which is encountered when surfaces are in relative motion with packed abrasives [18]. Higher carbon content means higher resistance to low-stress abrasion, although carbide particle size also has a strong influence. In addition, cobalt alloys resist wear due to their ability to absorb energy through the fcc to hcp transformation and through twinning [22].

Previous studies on the sliding wear resistance of cobalt-based alloys [1,3,7,11,22,23] found that the alloys suffered sliding wear with oscillating coefficient of friction. However, this oscillation was from experimental anomalous behaviour [11]. The coefficient of friction for these materials was within the range 0.1–0.25, and there was no correlation between the coefficient of friction and the amount of wear experienced.

The sliding wear behaviour of iron-, nickel- and cobalt-based alloys and coatings has received an extensive research attention. While many researchers have studied the effect of ruthenium (Ru) additions on hard metals, focusting on wear and corrosion resistance, hardness and toughness [24–32], there has been a limited research on the effect of minor additions of Ru to cobalt-based alloys. Thus, the purpose of this study was to investigate the wear rates and understand the wear behaviour of two different cobalt-based commercial alloys (ULTIMET^{TM} and STELLITE^{TM} 6B) and coatings modified with minor additions of Ru (ULTIMET^{TM} and STELLITE^{TM} 6, each with 0, 0.3 and 0.6 wt% Ru) on mild steel substrates. The additions of minor Ru content is intended to enhance the hardness of the cobalt-based coatings. Testing was by ball-on-disc sliding wear and hardness tests, which revealed that increased concentration of Ru in the coatings caused higher hardness, attributed to solid solution strengthening [24,25]. This, in turn, resulted in lower wear rates. The best performing STELLITE^{TM} 6 with 0.6 wt% Ru alloy that may potentially protect mild steel pump components from effects of wear was selected.

2. Materials and experimental methods

2.1. Materials

The materials studied were ULTIMET^{TM} and STELLITE^{TM} 6B (Table 1), supplied as bars by Multi Alloys, South Africa. The coatings were produced by mixing ULTIMET^{TM} and STELLITE^{TM} 6 powders (supplied by Weartech Pty (Ltd) and Fe Powder Supplies (Pty) Ltd, South Africa), each with zero or 0.3 or 0.6 wt% Ru additions (Table 1). The selection of 0.3 and 0.6 wt% Ru compositions for comparison with no Ru composition was deliberate, aimed at ensuring that ruthenium had no deleterious effect on the electrochemical and mechanical properties. These quantities were intentionally kept small, as ruthenium has proven effectiveness in small amounts [33], and they were considered sufficient to discern their distinct effects. The powders were thermally sprayed on to ASTM A516 mild steel substrates by the high velocity oxygen fuel (HVOF) technique, using a FANUC® System R-J3iB connected to a FANUC robot R-200 iA 16SF with the parameters in Table 2. Prior to HVOF spray coating, the mild steel substrates were pre-treated by removing any rust with acetone and grit-blasted using 20 grit abrasive to enhance good adhesion of the coating to the substrate. A digital pyrometer was used to control the temperature throughout the spray coating process.

2.2. Powder characterisation prior to thermal spraying

The particle sizes and distributions of the powders were determined by a MS 200 Malvern Mastersizer® analyser, with water as the dispersant. The powders were placed on to aluminium stubs with conductive double-sided carbon tape to examine their sizes and morphologies using SEM-EDX analysis. The powders were analysed by X-ray diffraction using a Panalytical X'pert Pro Diffractometer with Co-K_α radiation, at angles $2\theta = 0$–120°, and the data were interpretated using Panalytical Highscore Plus analytical software.

Table 1
Compositions of ULTIMET^{TM} and STELLITE^{TM} 6B and ULTIMET^{TM} and STELLITE^{TM} 6 powder for coatings and ASTM A516 mild steel substrate [12,13,33,34].

Alloy	Composition (wt%)											
	Co	Ni	Cr	Mo	W	Mn	Fe	Si	C	N	V	Cu
ULTIMET^{TM}-bulk [13]	Bal.	9.0	25.0	5.0	2.0	0.8	3.0	0.3	0.1	0.1	–	–
STELLITE^{TM} 6B bulk [12]	Bal.	2.6	28.8	1.5	4.5	1.0	2.5	1.3	1.2	–		–
ULTIMET^{TM} powder [13]	Bal.	9.0	26.0	5.0	2.0	0.8	3.0	0.3	0.1	0.1	–	–
STELLITE^{TM} 6 powder [34]	Bal.	2.5	30.0	1.5	4.0	1.4	3.0	0.7	1.0	–		
ASTM A516 Mild steel [33]	–	–	0.2	–	–	1.3	Bal.	0.3	0.2	–	0.1	0.2

Table 2
Operating parameters of the HVOF spraying processes [33].

Parameter	Value
Spraying distance (mm)	380
N_2 flow rate, as powder carrier ($m^3 \cdot h^{-1}$)	52
O_2 flow rate ($m^3 \cdot h^{-1}$)	56.6
Mesh size (μm)	–66.23 to + 22
Powder feed rate ($g \cdot s^{-1}$)	2.5
Spray gun speed ($cm \cdot s^{-1}$)	28
Substrate thickness (mm)	12
Torch velocity ($m \cdot s^{-1}$)	1500
Robot speed ($mm \cdot s^{-1}$)	300
Spray angle (°)	90
Substrate preheating temperature (°C)	47

2.3. Microstructure, X-ray diffraction and hardness testing

For elemental compositions, phase identification and hardness testing, ULTIMET™ and STELLITE™ 6 coatings, bulk alloys, and mild steel were cut, hot mounted in resin and wet ground from 80 to 1200 silicon carbide papers and 9 μm diamond paste, then polished on polishing cloths using 6, 3 and 1 μm diamond paste. The surfaces were cleaned in de-ionised water and degreased with acetone. The alloys were etched electrolytically in 100 mL HCl and 5 mL H_2O_2 (30 %) at 10 V DC for 5 s. Microstructures of the coatings were revealed without etching. The bulk alloys and the coatings were studied using a Carl Zeiss Sigma field emission scanning electron

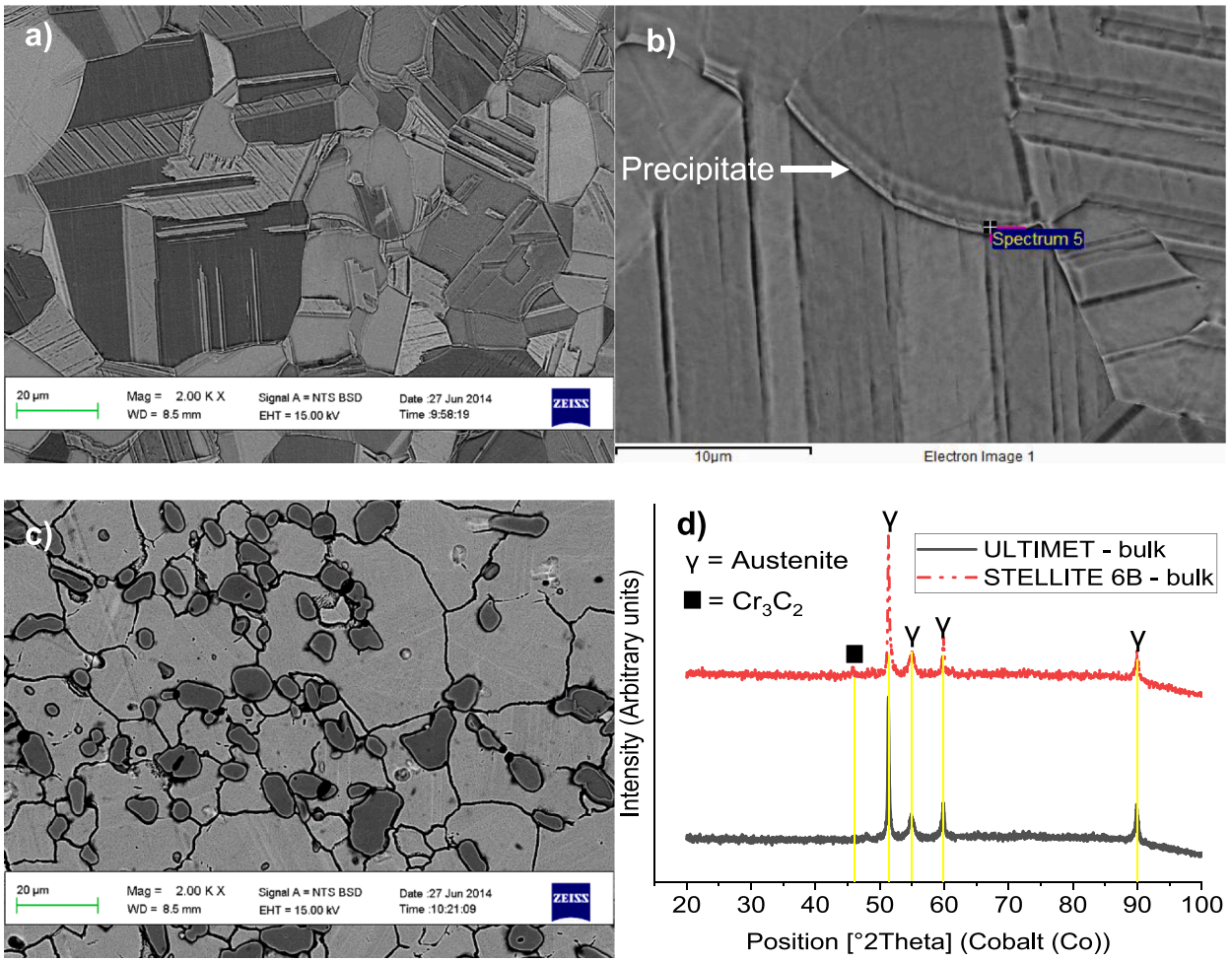


Fig. 1. SEM-BSE micrographs of the alloys: a) ULTIMET™, showing γ grains and twins, b) a higher magnification micrograph of ULTIMET™, showing narrow grain boundary precipitates [33], c) STELLITE™ 6B, showing twins in the γ grains and carbides in the matrix and at the grain boundaries, and d) XRD patterns of the alloys, showing γ-austenite and Cr_3C_2 phases [33].

microscope with energy dispersive X-rays spectroscopy (SEM-EDX) before and after the wear tests. Five EDX spot analyses were taken per phase, and the average was derived. The phases were identified by X-ray diffraction (XRD) using a Bruker D2 Phaser® diffractometer, with Fe filtered Co-K_α radiation at 30 kV, 10 mA at 2θ angles of 0–120°, scan rate of 1.2°min^{-1} and step size of 0.02° 2θ for bulk alloys and coatings. The grain sizes and the carbide proportions of the alloys were measured by the line intercept method on micrographs of 1000X, with at least 20 different placements. Hardness tests were performed using a Vickers FM-700 hardness tester, with 3 kg loads and a dwell time of 10 s. The tests were carried out five times, and the average was recorded.

2.4. Sliding wear tests

ULTIMET™, STELLITE™ 6B and mild steel alloys and the ULTIMET™ and STELLITE™ 6 coated samples were prepared metallographically as before (see section 2.3), ultrasonically cleaned in ethanol and air dried before each test. The ball-on-disk tests were done against 6 mm diameter 100Cr6 steel balls using a CSM Tribometer (in accordance with the ASTM G99-17 [35]), and carried out in duplicate for each composition at 23.2 ± 0.1 °C and 54 % humidity in unlubricated conditions. The test parameters were 0.21 m·s^{-1} linear speed, 200 m sliding distance, and 5 N and 10 N applied loads and were set in the CSM TriboX software for *in situ* measurement beforehand.

The sliding wear test parameters were chosen since they represent typical slurry pump components operating conditions [36]. Testing at these conditions helps evaluate the durability and wear resistance of the components operating where a good hardness and wear resistance is required.

A Nikon SMZ745 stereoscopic microscope and Carl Zeiss Sigma field emission SEM with EDX were used to investigate the wear mechanisms and measure the compositions of features in the wear tracks. The wear tracks were measured, to determine the worn volume (V_s in mm^3), by measuring outer (R_2) and inner (R_1) radii of the wear track, and the maximum penetration depth of the ball into the sample, P_{dmax}. V_s was calculated using Equation (1) [33]:

$$V_s = \pi\left(R_2^2 - R_1^2\right)P_{dmax} \tag{1}$$

The wear rate k (in $mm^3{\cdot}N^{-1}{\cdot}m^{-1}$) was calculated using Equation (2) [19]:

$$k = \frac{V_s}{W\hat{A}\cdot S} \tag{2}$$

where W = normal applied load (in N) and S = sliding distance (in m).

3. Results

3.1. Bulk alloys

The SEM-BSE micrographs of the ULTIMET™ and STELLITE™ 6B alloys before the wear tests are shown in Fig. 1. The microstructure of ULTIMET™ (Fig. 1 a) comprised well-defined austenite grains (γ, the cobalt-rich solid solution with Cr) with twins and Cr_3C_2 in the matrix and at grain boundaries (Fig. 1 b). STELLITE™ 6B (Fig. 1 c) also had austenite (γ) grains with some barely discernible twins and precipitates at the grain boundaries, confirmed by XRD (Fig. 1 d). Both ULTIMET™ and STELLITE™ 6B alloys showed typical annealed microstructures.

Within the scatter, the grain sizes were similar: 18.7 ± 6.0 μm for ULTIMET™ and 20.5 ± 2.0 μm for STELLITE™ 6B. EDX analyses of the alloys in Table 3 showed ULTIMET™ had Co and Cr as major constituents, with minor amounts of Ni, Mo, Fe and W. STELLITE™ 6B had similar major components as ULTIMET™, but with W and no Ni and Mo (Table 3). Although both alloys had Co and Cr, the proportions were different: ULTIMET™ had more Co and STELLITE™ 6B had more Cr. STELLITE™ 6B had O and Si in the matrix. Carbon was found in the precipitates in both alloys, confirming them as carbides, and the carbides had a volume fraction of 16 ± 1.5 % for STELLITE™ 6B (Fig. 1 c), while the precipitates for ULTIMET™ were narrow grain boundary precipitates (Fig. 1 b), which were too small to measure accurately for both composition and phase proportions, although they had more carbon than the matrix (Table 3).

Table 3
EDX analyses (wt%) of ULTIMET™ and STELLITE™ 6B alloys before wear tests [33].

Element	ULTIMET™ phase (wt%)			STELLITE™ 6B phase (wt%)		
	Overall	Matrix	Grain boundary precipitate	Overall	Precipitate	Matrix
C	3.5 ± 1.0	1.4 ± 0.6	6.0 ± 1.6	7.6 ± 0.0	10.5 ± 0.2	3.2 ± 0.2
Cr	24.4 ± 0.2	24.8 ± 0.3	23.8 ± 0.4	29.5 ± 1.0	75.3 ± 0.3	25.0 ± 0.0
Mn	0.8 ± 0.1	0.9 ± 0.1	0.9 ± 0.1	1.5 ± 0.1	1.3 ± 0.1	1.6 ± 0.1
Fe	2.8 ± 0.0	2.9 ± 0.1	2.8 ± 0.0	1.7 ± 0.1	0.6 ± 0.0	2.0 ± 0.0
Co	52.2 ± 1.0	53.3 ± 0.3	50.6 ± 0.7	46.2 ± 0.1	9.4 ± 0.2	54.3 ± 0.2
Ni	8.7 ± 0.1	8.8 ± 0.2	8.4 ± 0.2	1.7 ± 0.1	–	2.1 ± 0.1
Mo	5.4 ± 0.0	5.4 ± 0.1	5.2 ± 0.3	–	–	–
W	2.2 ± 0.0	2.4 ± 0.1	2.4 ± 0.1	4.8 ± 0.1	3.0 ± 0.3	5.7 ± 0.1

3.2. Particle sizes and surface morphologies of the powders

The average values for the particle size distributions of the powders showed ruthenium had highest mean particle size (573.4 ± 1.0 μm), followed by STELLITE™ 6 (49.1 ± 0.3 μm) and then ULTIMET™ (40.1 ± 0.1 μm). The size distributions of the powders are given in **Figure S1** (in Supplementary information). ULTIMET™ **(Figure S1 a)** and STELLITE™ 6 (**Figure S1** b) had narrow particle distributions, while Ru (**Figure S1** c) had a wider and bi-modal distribution due to agglomeration, and there was even a small peak for very fine particles. The peaks for the ruthenium powders were finest and least ~ 15 μm; middle ~ 18 μm; largest and most ~ 700 μm.

The powders are shown in Fig. 2. ULTIMET™ (Fig. 2 a) and STELLITE™ 6 (Fig. 2 b) powders were mainly spherical, while the ruthenium powder was angular, sometimes in plates of different sizes (Fig. 2 c) and agglomerated. When mixed with ruthenium, the smallest particles of ULTIMET™ and STELLITE™ 6 powders were enclosed by ruthenium powder.

3.3. Energy dispersive X-ray and X-ray diffraction results of the powders

Table 4 shows almost similar EDX results of the major components for both powder and coated samples. ULTIMET™ powder had Co and Cr as major constituents, with minor amounts of Ni, Mn, Mo, W, Si and Ru. STELLITE™ 6 had similar compositions, but with little Ni and slightly more W than ULTIMET™. Ruthenium was only found in nominal 0.6 wt% Ru ULTIMET™ and STELLITE™ 6 powders (possibly due to sampling errors) and all ULTIMET™ and STELLITE™ 6 coatings. The loss of ruthenium in the other coatings could have been due to the high melting point of Ru (~2334 °C), which meant it could have been left behind by HVOF and also due to separation during powder feeding, because ruthenium has a high density (12.27 g·cm^{-3}) [27,37,38].

The XRD patterns of powders of ULTIMET™ (Fig. 3 a) and STELLITE™ 6 (Fig. 3 b) showed that with and without Ru, there was mostly γ with Cr_3C_2.

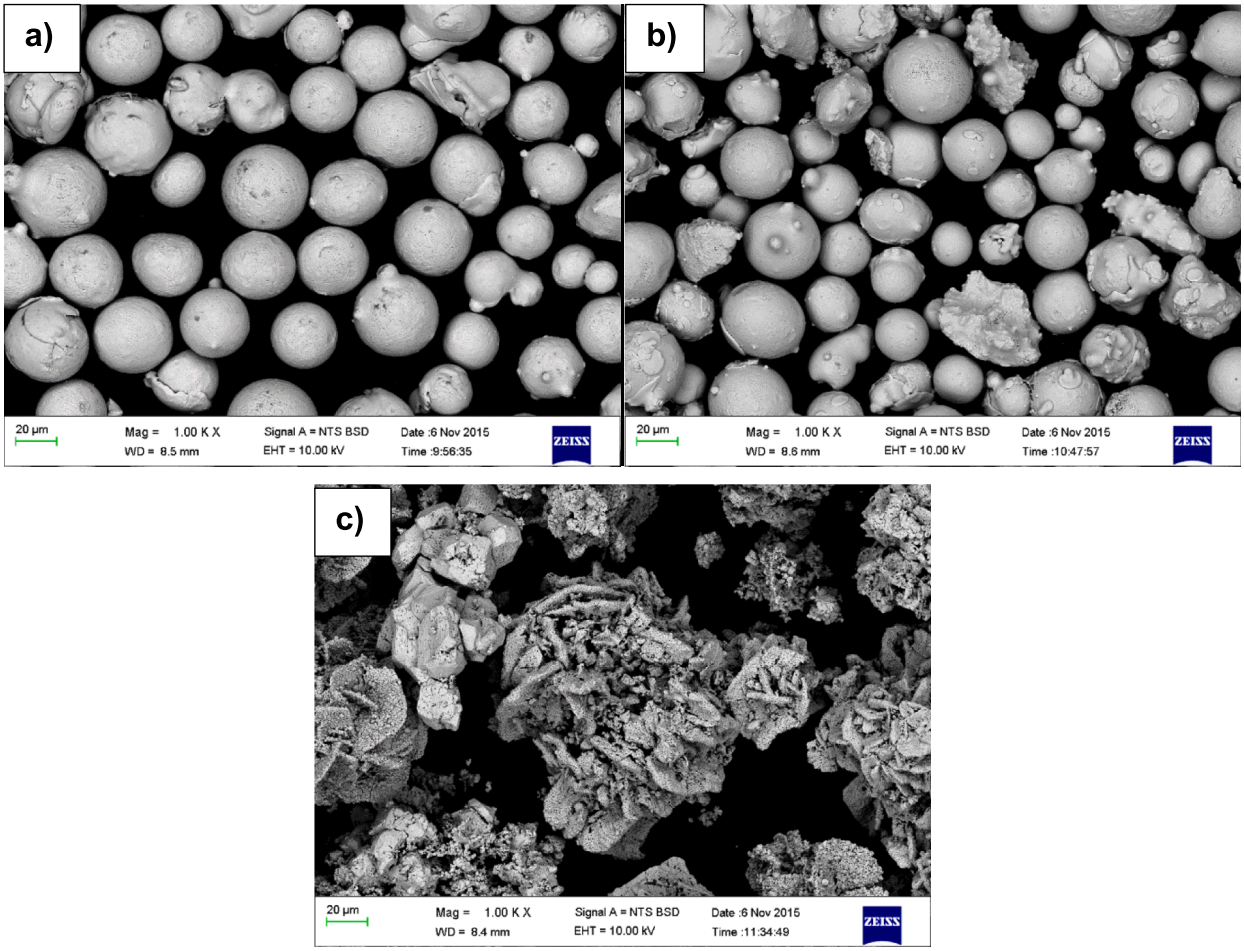


Fig. 2. SEM-BSE images showing powders of: a) ULTIMET™ [33], b) STELLITE™ 6 nominal 0.6 wt% Ru [33], and c) ruthenium [33].

Table 4
EDX analyses of the ULTIMET™ and STELLITE™ 6 powders and coatings.

Sample		Composition (wt%)									
		C	Si	Cr	Mn	Fe	Co	Ni	Mo	Ru	W
Powder	ULTIMET™ – 0 Ru	–	0.4 ± 0.0	31.0 ± 0.4	4.5 ± 1.0	–	46.7 ± 1.0	12.0 ± 1.0	3.6 ± 0.2	–	1.6 ± 0.2
	ULTIMET™ – 0.3 Ru	–	0.4 ± 0.0	32.0 ± 1.0	4.0 ± 1.0	–	47.0 ± 1.0	11.7 ± 1.0	3.0 ± 1.0	–	1.7 ± 0.0
	ULTIMET™ – 0.6 Ru	–	0.4 ± 0.1	31.0 ± 1.0	3.4 ± 1.0	–	47.0 ± 1.0	12.0 ± 1.0	3.2 ± 1.0	1.0 ± 0.0	1.7 ± 0.2
	STELLITE™ 6–0 Ru	–	0.9 ± 0.0	35.0 ± 1.0	2.7 ± 2.0	–	55.0 ± 2.0	4.4 ± 0.0	0.2 ± 0.0	–	4.0 ± 0.0
	STELLITE™ 6–0.3 Ru	–	0.7 ± 0.0	31.0 ± 2.0	6.0 ± 1.0	–	55.0 ± 2.0	3.8 ± 0.0	0.3 ± 0.1	–	2.6 ± 0.1
	STELLITE™ 6–0.6 Ru	–	0.7 ± 0.1	31.0 ± 1.0	5.6 ± 1.0	–	55.0 ± 2.0	3.6 ± 0.0	0.2 ± 0.0	1.5 ± 0.0	2.6 ± 0.0
Coating	ULTIMET™ – 0 Ru	1.7 ± 0.0	0.3 ± 0.0	28.0 ± 1.0	1.0 ± 0.0	0.2 ± 0.0	50.0 ± 0.0	13.0 ± 1.0	4.5 ± 0.0	–	2.0 ± 0.0
	ULTIMET™ – 0.3 Ru	1.3 ± 0.0	0.2 ± 0.0	29.0 ± 1.0	0.8 ± 0.0	0.6 ± 0.2	52.0 ± 1.0	12.0 ± 0.0	4.0 ± 1.0	0.3 ± 0.0	2.0 ± 0.0
	ULTIMET™ – 0.6 Ru	1.7 ± 0.0	0.3 ± 0.0	29.5 ± 0.0	0.8 ± 0.0	–	48.8 ± 0.0	12.3 ± 0.0	4.5 ± 0.0	0.2 ± 0.0	2.0 ± 0.0
	STELLITE™ 6–0 Ru	2.7 ± 1.0	0.7 ± 0.0	33.1 ± 1.0	2.3 ± 1.0	–	53.0 ± 1.0	3.4 ± 1.0	0.4 ± 0.0	–	4.2 ± 0.0
	STELLITE™ 6–0.3 Ru	2.7 ± 0.0	0.7 ± 0.0	30.0 ± 1.0	3.8 ± 1.0	0.1 ± 0.0	55.0 ± 1.0	3.4 ± 0.0	0.3 ± 0.0	0.2 ± 0.0	3.8 ± 0.0
	STELLITE™ 6–0.6 Ru	–	0.7 ± 0.0	30.5 ± 1.0	5.6 ± 1.0	–	55.2 ± 2.0	3.6 ± 0.0	0.2 ± 0.0	1.5 ± 0.0	2.6 ± 0.0

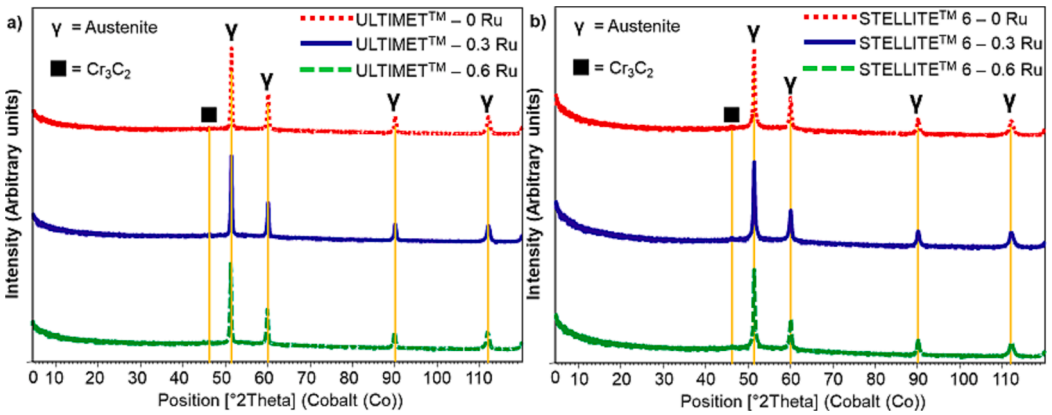


Fig. 3. XRD patterns of: a) ULTIMET™, and b) STELLITE™ 6 powders with 0, 0.3 and 0.6 wt% Ru, showing mainly γ and Cr_3C_2.

3.4. Microstructure, energy dispersive X-ray spectroscopy and X-ray diffraction of the coatings

The SEM-BSE surface micrographs of the ULTIMET™ and STELLITE™ 6 coatings with Ru additions before the wear tests are shown in Fig. 4. Nominal 0, 0.3 and 0.6 wt% Ru ULTIMET™ (Fig. 4 a–c) and STELLITE™ 6 (Fig. 4 d–f) had dendrites surrounded by a network of interdendritic carbides, although there were regions where the dendrites could not be discerned. Globular particles of both coatings are shown in Fig. 4, which were the original spherical particles or "splats" from thermal spraying of the source powders. The average splat size was 48.1 ± 9.8 μm. The ruthenium was not well distributed and was outside the splats. There were also pores, sometimes at the splat edges.

Table 4 shows the coatings were similar to the powders, so there was no contamination. Apart from STELLITE™ 6–0.6 Ru, all the coatings apparently had carbon, probably from the conductive double-sided carbon tape used to hold the samples for SEM-EDX analysis.

XRD patterns for all coatings (Fig. 5) were very similar with mainly γ, because they were all cobalt-based, and their compositions were similar.

3.5. Hardness measurements of the coatings and alloys

Fig. 6 shows the trend of hardness with different Ru contents for the ULTIMET™ and STELLITE™ 6 coatings, which increased when

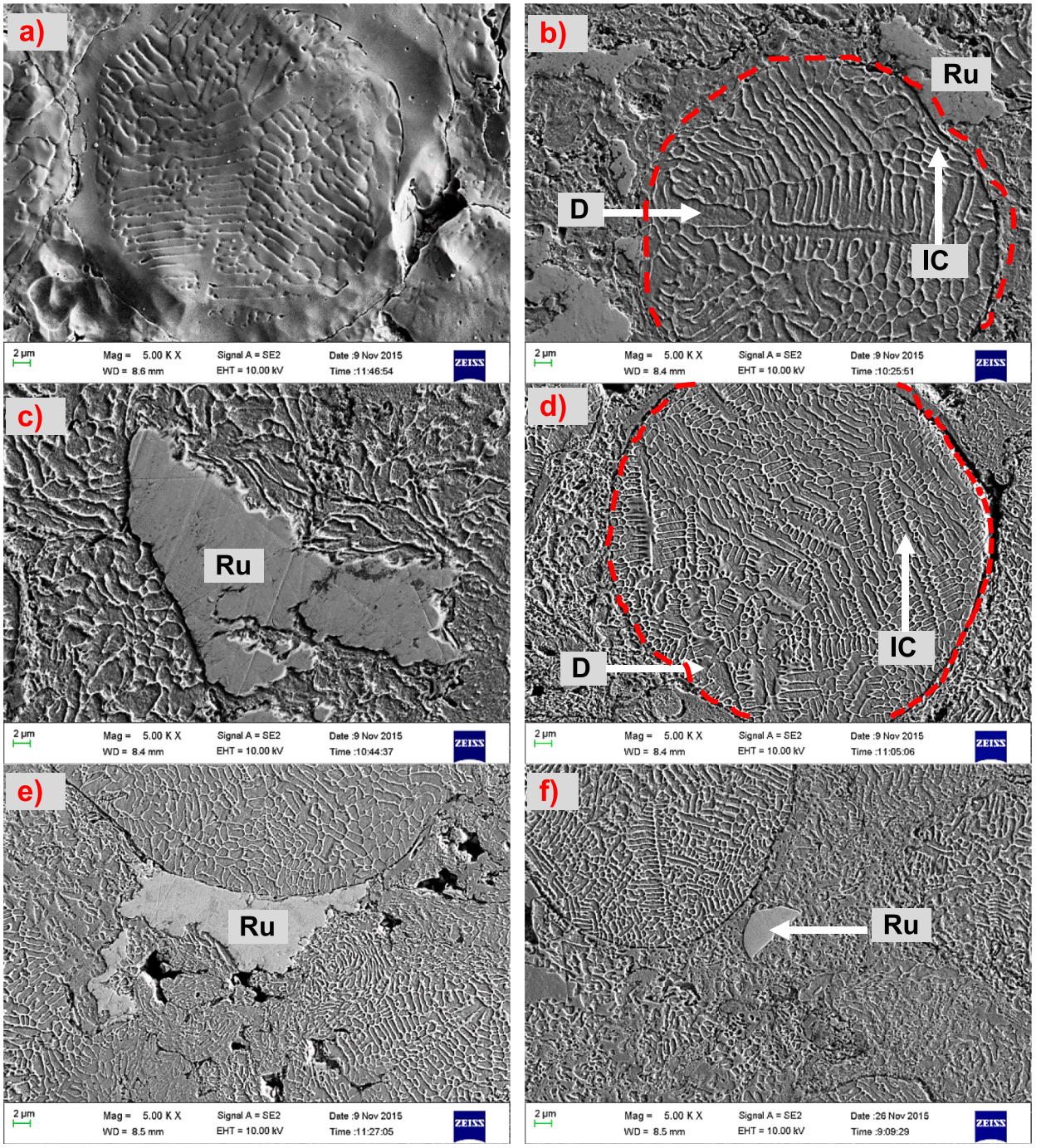


Fig. 4. SEM-SE micrographs showing the top surfaces of ULTIMET^{TM} coatings with: a) 0 Ru, b) 0.3 wt% Ru, and c) 0.6 wt% Ru and STELLITE^{TM} 6 coatings with: d) 0 Ru, e) 0.3 wt% Ru [33], and f) 0.6 wt% Ru, all with dendrites (D) and interdendritic carbides (IC).

Ru content was increased. The hardnesses of STELLITE^{TM} 6 bulk alloy and coatings were higher than the ULTIMET^{TM} bulk alloy and coatings. There were large errors, up to ± 39 HV_3 (Fig. 6), which is consistent with the inhomogeneity in the coatings, whereas the homogeneous mild steel substrate had an error of only of ± 5 HV_3.

3.6. Friction and sliding wear

The friction behaviour of mild steel, ULTIMET^{TM} and STELLITE^{TM} 6B bulk alloys and ULTIMET^{TM}, STELLITE^{TM} 6 coatings with no

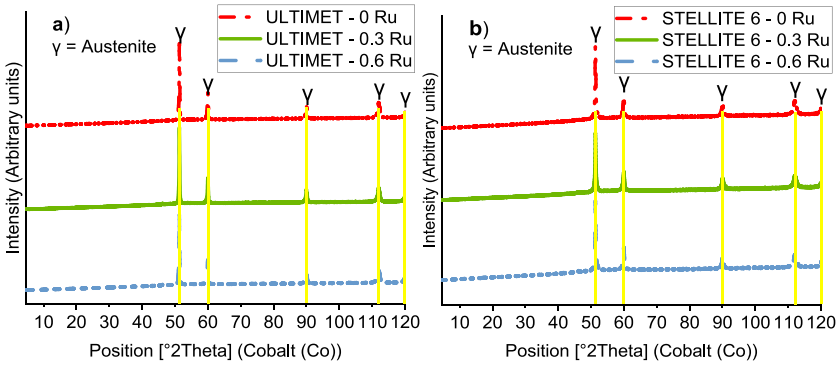


Fig. 5. XRD patterns of: a) ULTIMET™, and b) STELLITE™ 6 coatings, with 0, nominal 0.3 wt% Ru and nominal 0.6 wt% Ru, showing only fcc (γ).

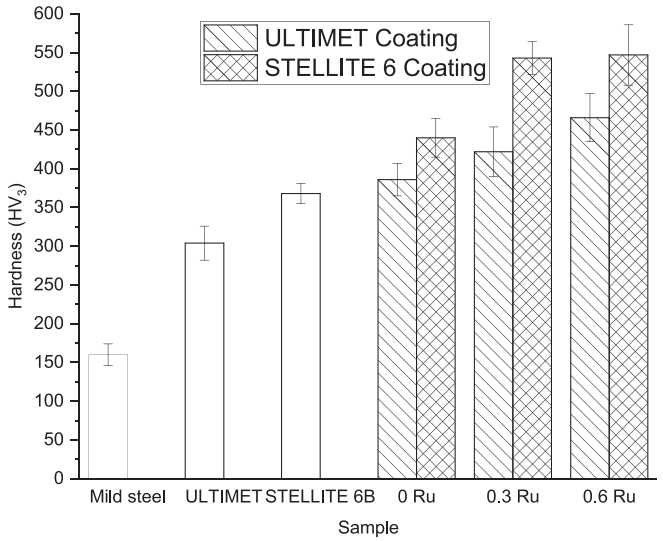


Fig. 6. Hardnesses (HV_3) of mild steel substrate, ULTIMET™ and STELLITE™ 6B bulk alloys, and nominal 0, 0.3 and 0.6 wt% Ru ULTIMET™ and STELLITE™ 6 coatings.

Ru, nominal 0.3 wt% Ru and nominal 0.6 wt% Ru sliding against 100Cr6 steel balls at 5 N as a function of sliding distance is given in Fig. 7 a and b). At the very beginning of the sliding test, the coefficients of friction (μ) of all samples varied greatly.

The friction behaviour of mild steel, ULTIMET™ and STELLITE™ 6 coatings with no Ru, nominal 0.3 wt% Ru and nominal 0.6 wt% Ru sliding against 100Cr6 steel balls as a function of sliding distance at 10 N is given in Fig. 7 c and d). At the 10 N load, the sliding behaviours were similar to those at 5 N although there was greater fluctuation and higher coefficients of friction at 10 N than at 5 N. The friction behaviour of ULTIMET™ and STELLITE™ 6B bulk alloys was also similar to those of the coatings. The coefficients of friction for each sample tested are given in Fig. 8, indicating higher coefficients of friction gave lower wear rates. The volume losses (Fig. 9 a and b) increased at higher loads to give higher wear rates (Fig. 9 c and d). Both STELLITE™ coatings and alloy had lower volume losses and wear rates than ULTIMET™ and mild steel at all loads. At both loads, STELLITE™ 6 – 0.6 Ru had the lowest wear rate (k), showing it was the best coating tested for applications where wear may be a problem.

As sliding occurred, the ball ploughed the surface of the bulk alloys, producing grooves. The sliding wear mechanisms for ULTIMET™ against the 100Cr6 ball gave irregular grooves at both loads (Fig. 10 a, Fig. 11 a and b), while in STELLITE™ 6B wear also gave grooves (Fig. 10 b, Fig. 11 c and d) filled with debris. The widest wear track with coarser grooves, and thus the highest volume loss, occurred on ULTIMET™ (Fig. 10 a) whereas STELLITE™ 6B (Fig. 10 b) was more resistant to sliding wear at both loads.

SEM micrographs also showed that ULTIMET™ had grooves and wear debris smeared onto the surface (Fig. 10 a), delamination (Fig. 11 a) and slip bands (Fig. 11 b) on the wear track. STELLITE™ 6B had debris in the grooves (Fig. 10 b and **11**c and d). Some of the matrix was removed, leaving carbides above the surface (Fig. 11 d). The grooves were more severe with increased load, and was the dominant wear mechanism for both alloys.

Table 5 shows the EDX analyses of ULTIMET™ and STELLITE™ 6B wear tracks from Fig. 10 a and b, Fig. 11 a and d after ball-on-disc sliding wear at 5 N and 10 N. Comparing the analyses before (Table 3) and after (Table 5) wear for ULTIMET™, the amounts of Mn and Ni increased, and C, Mo, Fe and W decreased, while Si (but < 1 wt%, so probably not accurate) and O were found after wear and

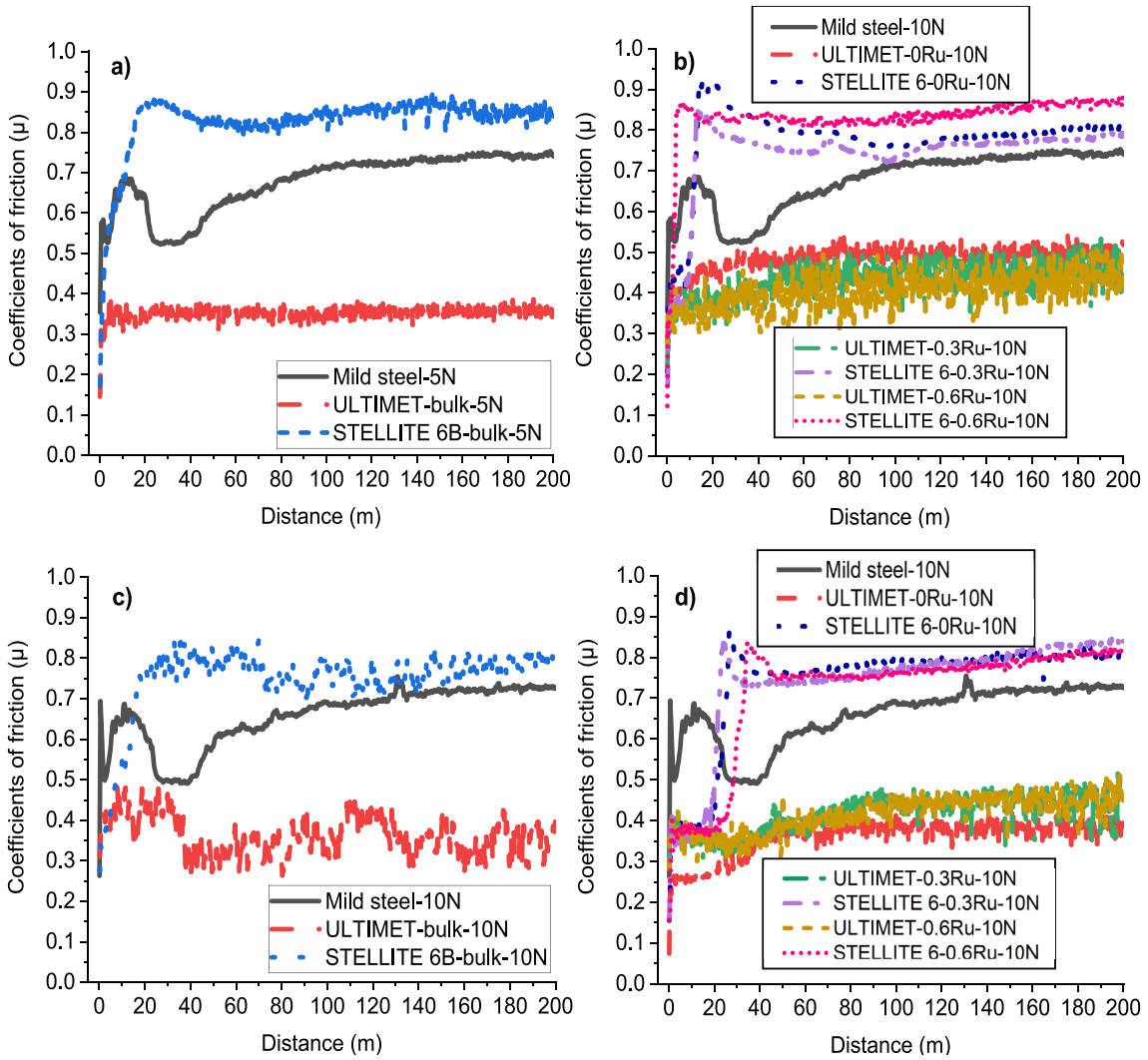


Fig. 7. Coefficients of friction of mild steel, ULTIMET^{TM} and STELLITE^{TM} 6B bulk alloys, and ULTIMET^{TM} and STELLITE^{TM} 6 coatings under dry sliding wear conditions against 100Cr6 steel balls at: a) and b) 5 N, and c) and d) 10 N loads [33].

the Co and Cr contents remained the same while no Fe found after wear. At position A (Fig. 10 a), which was smeared wear debris, the trends were the same, except that some Fe was left. For STELLITE^{TM} 6B, only Ni and Mn increased, while C, Cr, Co and W decreased after wear, while Mo (below 1 wt%, so was probably not accurate), O and Si (but < 1 wt%, so probably not accurate) appeared after wear. The loss of C and Cr after wear was because some Cr_3C_2 was lost, as shown by the holes in Fig. 11 d as some of the supporting matrix was lost by by ploughing (Figs. 10 and 11) (which reduced the Fe and Co). The oygen appeared because of the reaction with air, and slight increases of Ni was from the 100Cr6 balls.

Figs. 12 and 13 show morphologies of ULTIMET^{TM} and STELLITE^{TM} 6 coatings with 0, 0.3 and 0.6 wt% Ru and mild steel substrates after sliding against 100Cr6 steel balls at 5 N and 10 N. All samples showed predominantly abrasive wear, with grooves at both loads. The debris took part in three-body wear. ULTIMET^{TM} coatings (Figs. 12 and 13 a–c) had deep grooves, some large pits, smeared particles and debris, which increased at 10 N. ULTIMET^{TM} coatings with nominal 0.3 wt% Ru experienced smearing at both loads. STELLITE^{TM} 6 coatings (Figs. 12 and 13 d–f) had almost similar wear mechanisms to ULTIMET^{TM} coatings at both loads. In addition, STELLITE^{TM} 6 had more debris than ULTIMET^{TM} coatings. The mild steel (Fig. 12 g and **13** g) had deep grooves, which collected debris.

4. Discussion

4.1. Bulk alloys

All the bulk alloys were polycrystalline, with γ matrices and carbides. The bulk alloys had not been heat treated to optimise the microstructures, and solution treatment [39] followed by ageing [40], would have improved the microstructures. Thus, ULTIMET^{TM}

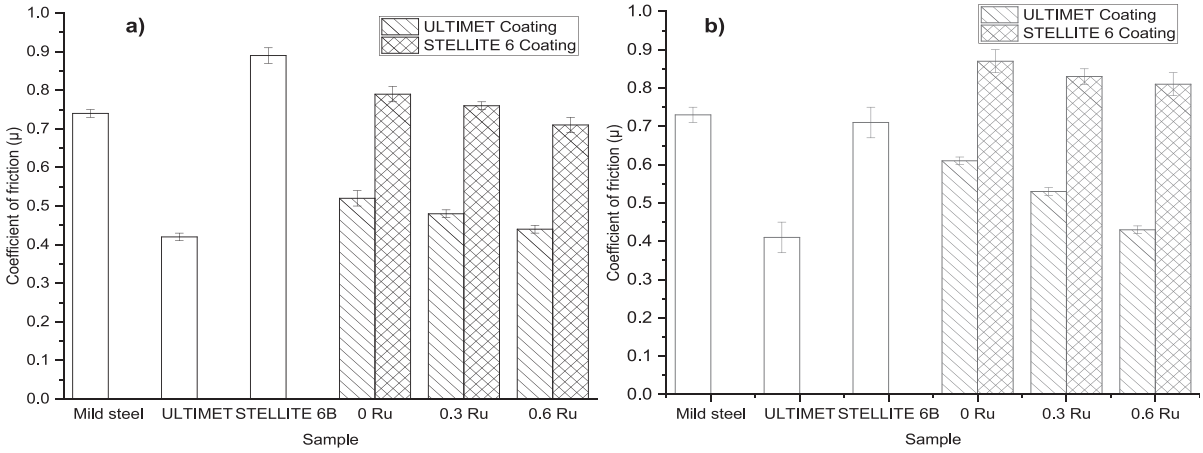


Fig. 8. Average coefficients of friction of mild steel, ULTIMET™ and STELLITE™ 6B bulk alloys, and ULTIMET™ and STELLITE™ 6 coatings at: a) 5 N, and b) 10 N loads [33].

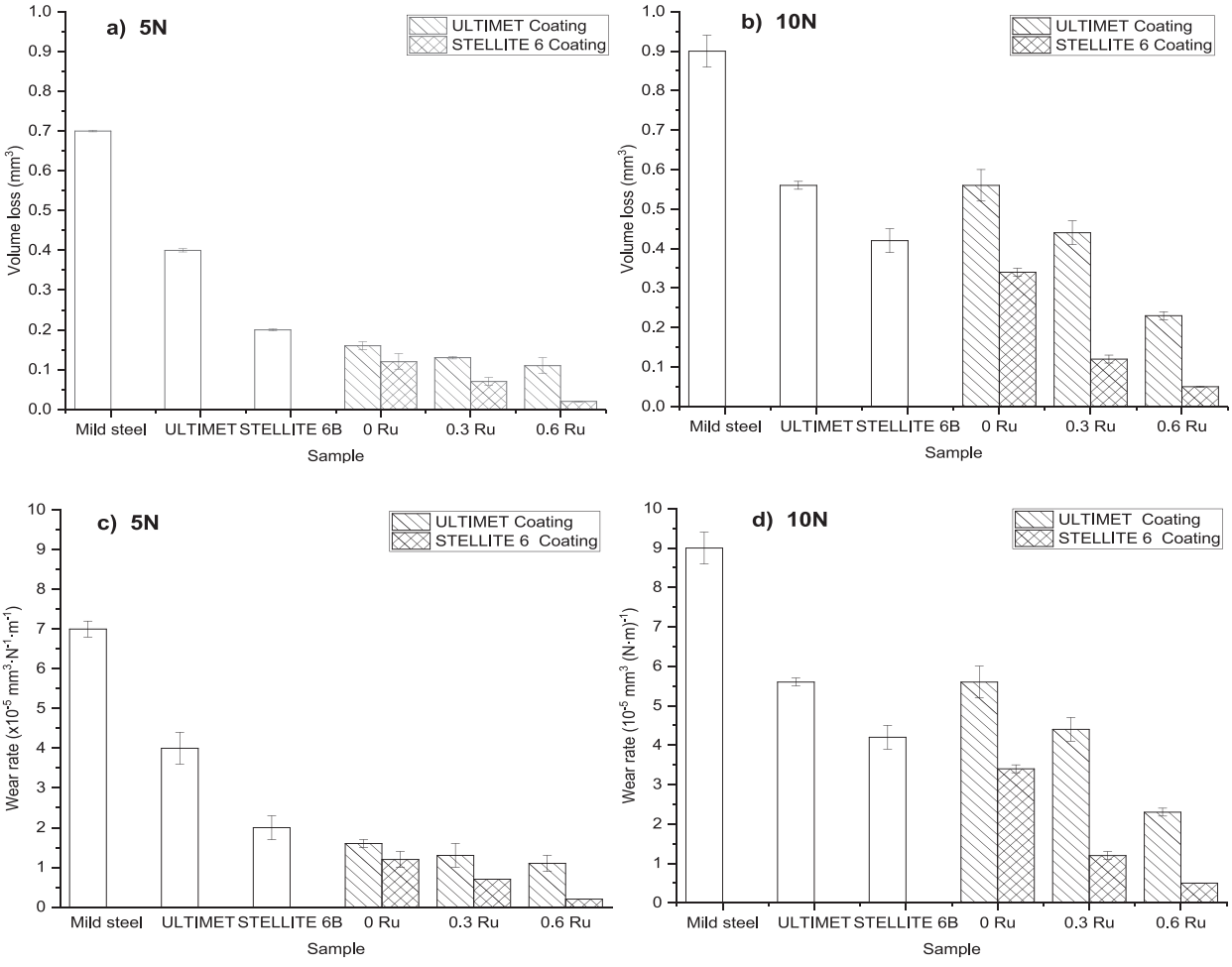


Fig. 9. Wear results for mild steel, ULTIMET™ and STELLITE™ 6B bulk alloys, and ULTIMET™ and STELLITE™ 6 coatings under sliding wear conditions: a) volume loss for 5 N load, b) volume loss for 10 N load, and c) wear rates for 5 N load, and d) wear rates for 10 N load.

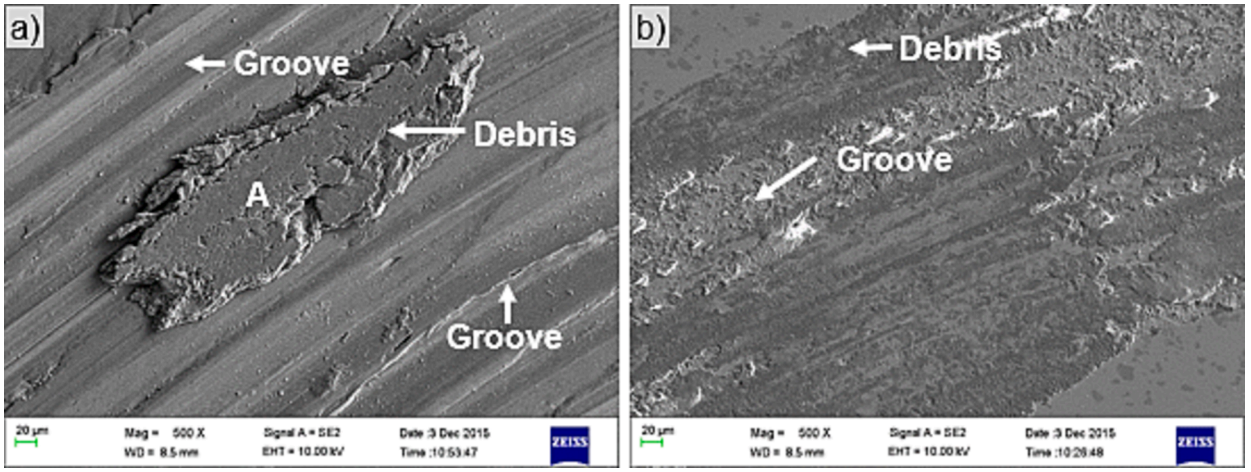


Fig. 10. SEM-SE micrographs after ball-on-disc sliding wear of: a) ULTIMET^{TM}, showing fairly long continuous grooves, and debris smeared on the surface (position A), and b) STELLITE^{TM} 6B, showing much debris on the wear track [33].

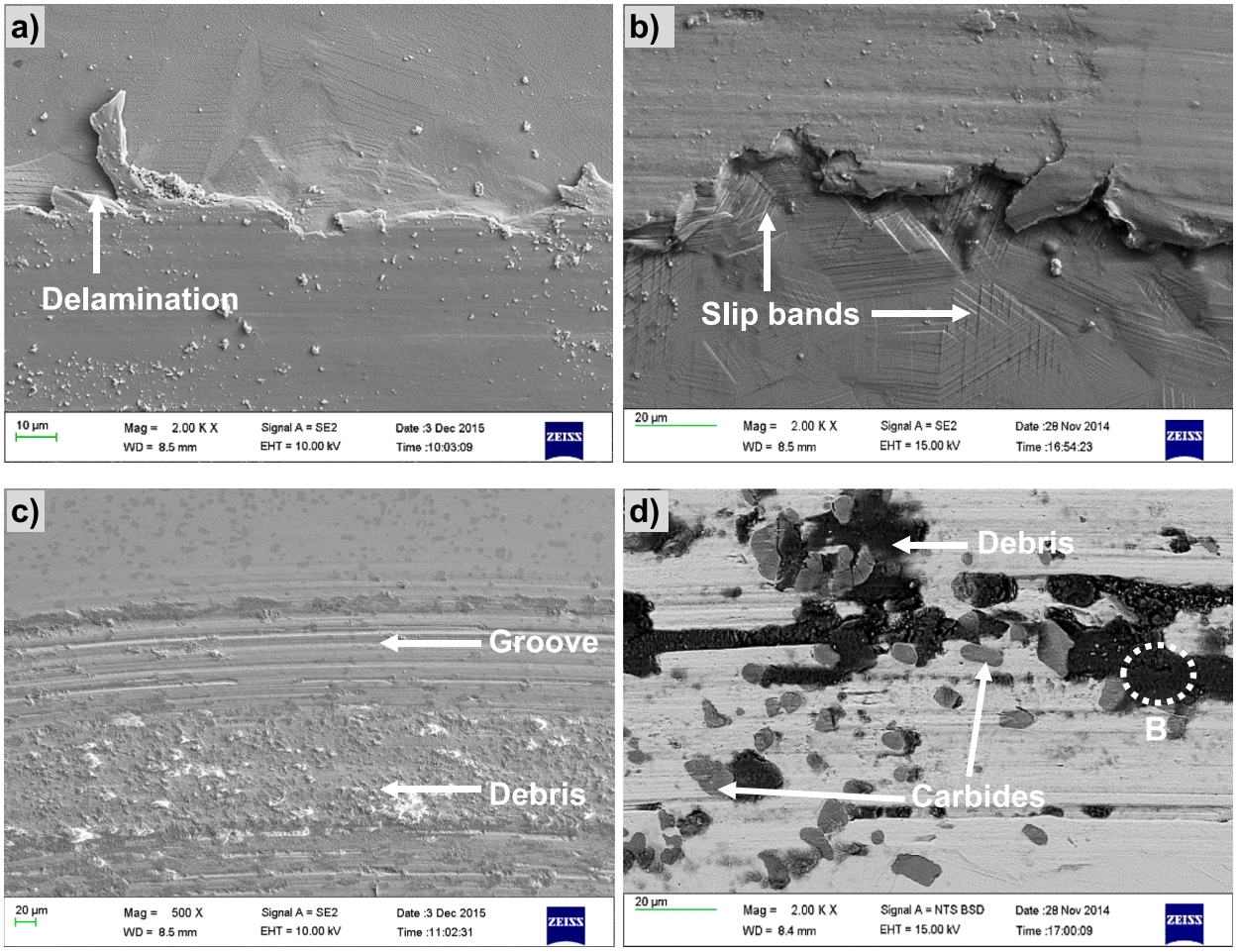


Fig. 11. SEM-SE micrographs of: a) and b) ULTIMET^{TM}, showing delamination, slip bands on the surface near the wear track and debris smeared over the grooves, c) SEM-SE and d) SEM-BSE micrographs of STELLITE^{TM} 6B, showing debris (position B), and the matrix phase removed, leaving carbides above the surface [33].

Table 5
EDX analyses of the ULTIMET™ and STELLITE™ 6B sample surfaces of Fig. 10 a and b after ball-on-disc sliding wear at 5 N [33].

Element (wt%)	ULTIMET™		STELLITE™ 6B	
	Overall	Position A	Overall	Position B
C	0.7 ± 0.0	0.8 ± 0.5	2.2 ± 0.0	1.7 ± 1.0
O	1.0 ± 0.1	9.6 ± 1.0	19.0 ± 1.0	25.5 ± 2.0
Si	0.2 ± 0.0	0.2 ± 0.0	0.2 ± 0.0	0.2 ± 0.0
Cr	24.8 ± 0.3	22.8 ± 1.0	27.1 ± 1.0	25.0 ± 2.0
Mn	3.0 ± 0.5	1.6 ± 0.0	8.0 ± 1.0	–
Co	52.3 ± 0.1	2.2 ± 0.0	37.0 ± 1.0	12.7 ± 2.0
Ni	12.6 ± 0.4	46.0 ± 0.0	3.3 ± 0.0	29.6 ± 4.0
Mo	3.6 ± 0.2	11.2 ± 1.0	0.5 ± 0.0	2.9 ± 0.0
W	1.6 ± 0.2	3.6 ± 0.0	2.5 ± 0.0	0.4 ± 0.0

could have carbides distributed more within the grains and less on the grain boundaries, and STELLITE™ 6B could have had finer grains.

4.2. Particle size distribution of the powders and microstructures of the coatings

Although ruthenium was not well distributed within the coatings (Fig. 4 b, c, e and f), the size of the ruthenium particles was similar to the middle peak of the powder distribution (**Figure S1** c). Thus, the agglomerations of the ruthenium powders were either broken down during thermal spraying and the finest particles possibly lost, or they went into solid solution in the matrix to an extent below that which was detectable by EDX.

The Ru content for nominal 0.6 wt% Ru was approximately half of what it should have been (~0.2 wt% Ru) for ULTIMET™, but 1.5 ± 0.0 wt% Ru for STELLITE™ 6. This could be due to Ru being lost during spraying of ULTIMET™ (although it was not lost for STELLITE™ 6). However, there was inhomogeneous distribution of the powders during mixing and spray coating, especially since Ru is heavy, which indicated that the ruthenium powder should be sieved and milled for a longer time prior to thermal spraying to give smaller particles.

Decreased grain size increases hardness [41,42]. A better distribution of the carbides would also have been beneficial, especially for STELLITE™ 6B, which had fairly large carbides both on the grain boundaries and within the grains, and ULTIMET™, which had its few carbides exclusively on the grain boundaries.

The dendritic microstructures for both ULTIMET™ and STELLITE™ 6 coatings occurred because the cobalt solid solution solidified first, with the carbides solidifying interdendritically afterwards [33].

Although the main primary focus of this study was assessing the sliding wear behaviour of the materials, surface roughness analysis was supposed to be conducted before sliding wear tests to explain the relationship between the coefficient of friction and wear resistance properties [43–45]. The coatings surfaces were prepared by polishing with diamond paste to achieve a 1 μm surface finish and then cleaned in de-ionised water and degreased with acetone. These steps ensured reasonably acceptable surface roughness for this study [46]. Another limitation of this study was the absence of cross-section microstructural analyses of the coatings, which could have provided insights into variations in the microstructures, wear mechanisms, and plastic deformation induced by sliding forces on the coatings [45,47,48]. Hence, for future research directions, it is recommended to include surface roughness and cross-sectional analyses to complement the findings of the study.

4.3. Hardness of the alloys and coatings

Each alloy matrix had its own inherent hardness, which would also have been affected by the grain sizes, and the carbide distribution would also have an effect. The carbides would improve wear resistance, as is known for STELLITE™ 6B [3,13,16]. ULTIMET™ had fewer carbides than STELLITE™ 6B (Fig. 1) since it had less carbon (Table 1) and no carbides such as Cr_7C_3, $Cr_{23}C_6$, WC and W_2C, because of the low carbon content. The higher hardness of the STELLITE™ 6B alloy than the ULTIMET™ alloy was due to the hard chromium-rich carbides [7,15,23]. Additionally, the higher tungsten content in STELLITE™ 6B may have also contributed for its higher hardness than ULTIMET™, and higher sliding wear resistance [10,21,23].

The absence of the Cr_7C_3 suggests that its formation was not favoured under the composition and temperature conditions during its production, the formation of such carbides was not favoured. This was likely because the primarily formed Cr_3C_2 phase could not further decompose into any other carbide phases within the matrix [49]. As a result, only the Cr_3C_2 phase was detected by XRD as shown in (Fig. 1 d).

The hardness of the ULTIMET™ and STELLITE™ 6B bulk alloys, ULTIMET™ and STELLITE™ 6 coatings is important in applications where wear resistance is needed, and the maximum in this study was for the STELLITE™ with Ru (547 ± 39 HV_3), which was higher than Haynes 6B and 25 alloys (310–466 HV_3) [23]. However, Ahmed *et al.* [3] reported a wider range: 419–704 HV_3 for STELLITE™ 6 and 20, while Antony [16] found Co-30Cr-12 W-2.5C to have higher hardnesses (510–620 HV_3), and lower hardness (230–390 HV_3) for Co-26Cr-7 W-2.8Ni-0.2C, Co-26Cr-7 W-Fe-0.2C, Co-26Cr-5Mo-2.8Ni-0.2C and Co-26Cr-5Mo-Fe-0.2C (wt%) alloys. An *et al.* [4] studied hardness evolution in cobalt alloys, although with very lower hardness evolution (200–280 HV_3) than the ULTIMET™ (386 ± 21–466 ± 41 HV_3) and STELLITE™ 6 (440 ± 25–547 ± 39 HV_3) coatings, where hardness was due to martensite

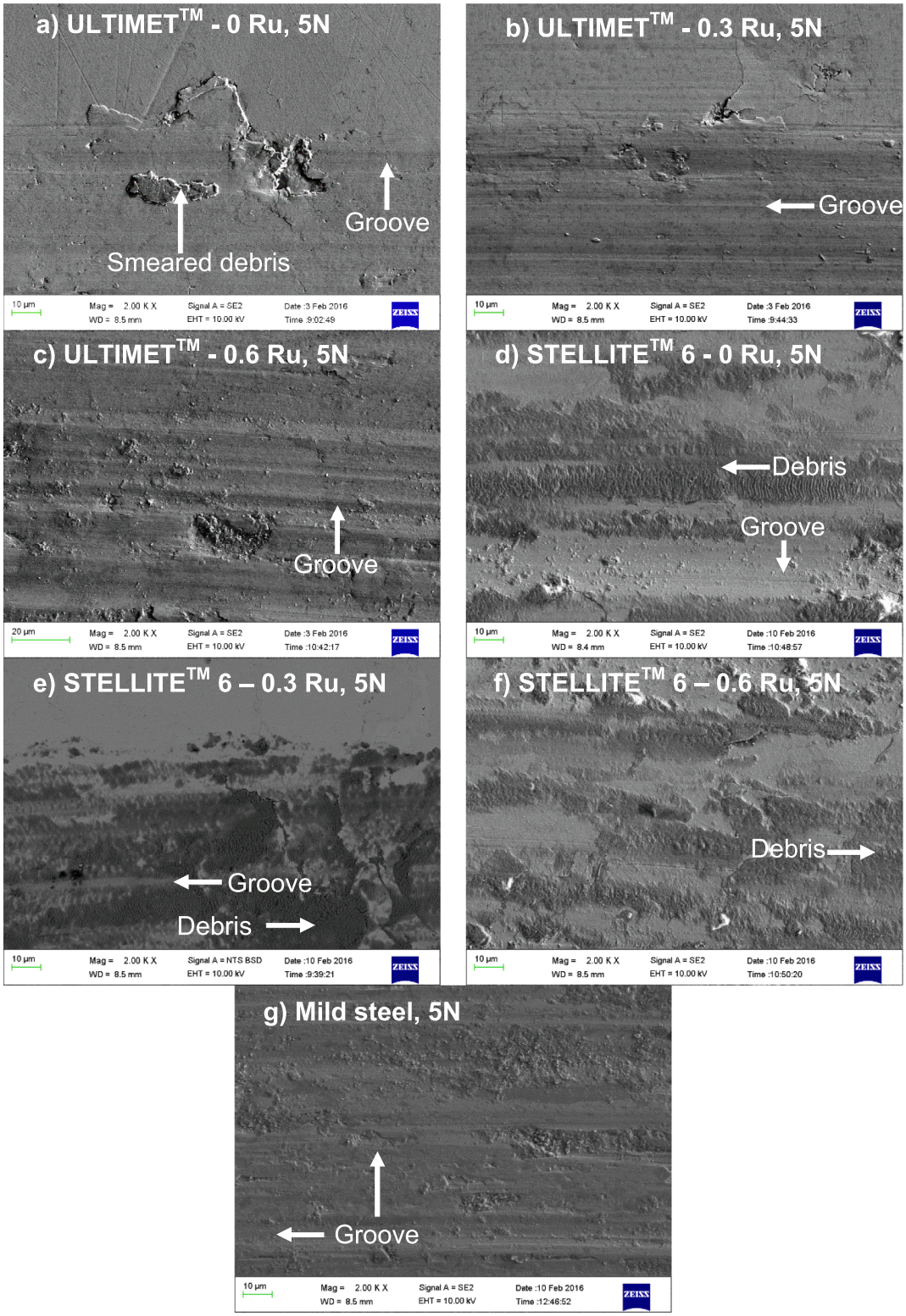


Fig. 12. SEM-SE micrographs of: a)–c) ULTIMET™ and d)–f) STELLITE™ 6 coatings and g) mild steel after dry sliding wear conditions against 100Cr6 steel balls at 5 N [33].

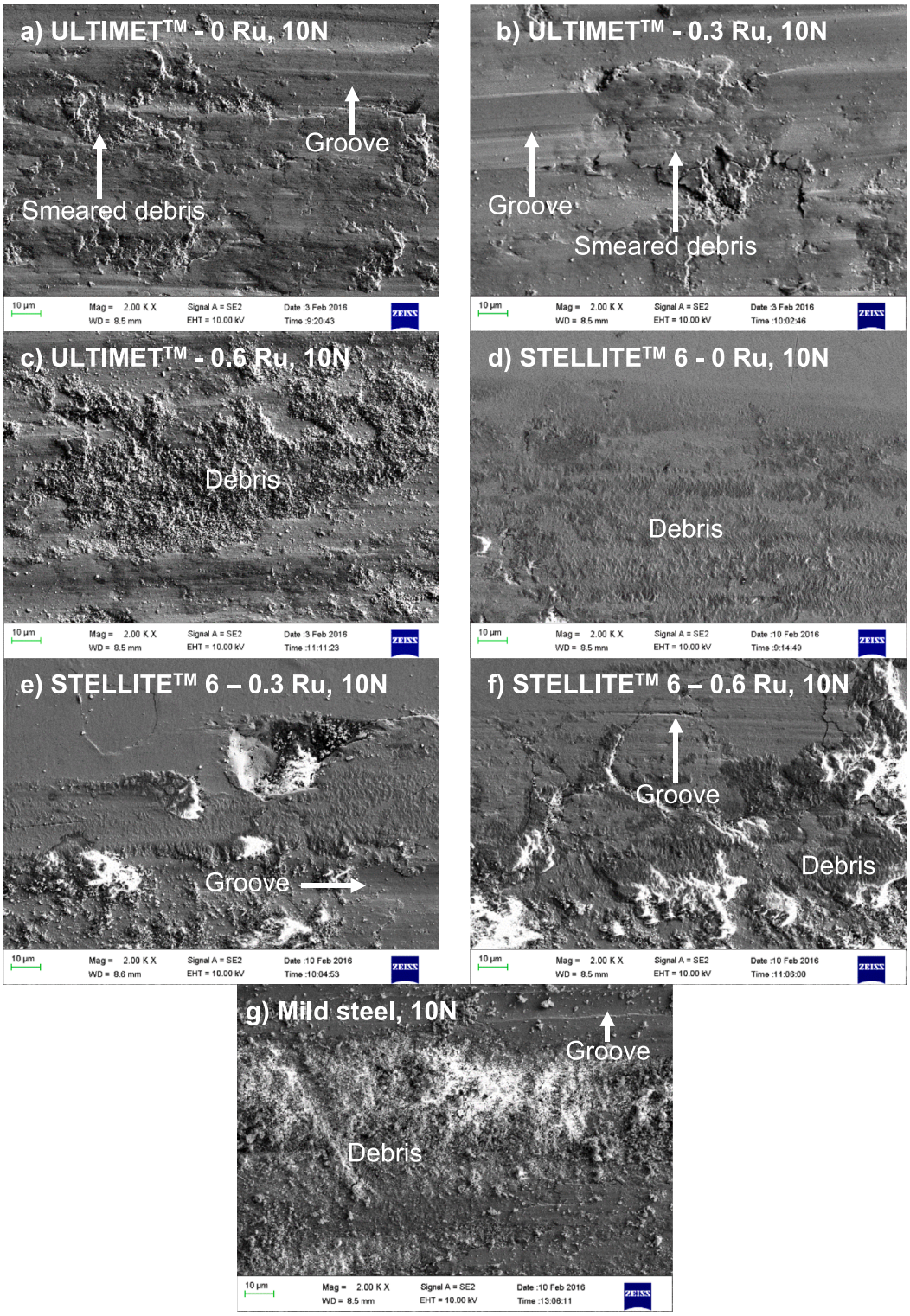


Fig. 13. SEM-SE micrographs of: a)–c) ULTIMET™ and d)–f) STELLITE™ 6 coatings, and after dry sliding wear conditions against 100Cr6 steel balls at 10 N [33].

and mechanical twins formed during cold rolling.

4.4. Effect of ruthenium on hardness of the coatings

Ruthenium exhibits a tendency to form solid solutions with cobalt or other elements, potentially leading to the creation of stronger intermetallic phases. However, XRD results only revealed the presence of γ-austenite and Cr_3C_2 (Fig. 5), with no detection of other carbides such as Cr_7C_3 or $Cr_{23}C_6$. An increase in the amount of ruthenium to the coatings resulted in higher hardness values (Fig. 6). This can be attributed to solid solution strengthening, which led to lower wear rates due to a solid solution strengthening, resulting in lower wear rates (Fig. 9) [24,25,50]. However, a significant amount of the ruthenium occurred as islands in the microstructure and did not contribute to a large extent to the solid solution.

Although ruthenium increased the hardness of both ULTIMET™ and STELLITE™ 6 coatings, the larger errors than for the coatings without Ru were probably due to poor distribution of Ru within the coating. This probably occurred because of the inhomogeneous distribution of Ru particles (due to the powder particle size range) during mixing and thermal spraying, giving unequal distributions of Ru [33] in the coatings (Fig. 4 b, c, e and f). The 0.6 wt% Ru ULTIMET™ coating had the highest hardness of the ULTIMET™ coatings (Fig. 6). The 0.3 wt% Ru and 0.6 wt% Ru STELLITE™ 6 coatings had equally the highest hardness, thus 0.3 wt% Ru may be the optimum addition for these coatings considering both performance and cost.

The higher hardnesses of the STELLITE™ 6 coatings were due to the presence of Cr_3C_2 and higher Cr content which improved wear resistance [7,51]. The higher C and W contents of STELLITE™ 6 than ULTIMET™ could have also formed tungsten carbides [16,52] (although if present, these were not observed) and thus a higher overall hardness. Although carbides were visible in the microstructures of the splats (Fig. 4), they had insufficient volume to be detected by XRD (Fig. 5). The carbide distribution was also inhomogeneous, as well as the Ru distribution, thus the coating process needs to be optimised and sections through the coatings need to be studied to ascertain the homogeneity with coating depth.

In many industrial applications where wear resistance is needed, a material with a good hardness is required. As shown in Table 1, STELLITE™ 6 coatings and STELLITE™ 6B alloy have more carbon and chromium than ULTIMET™ coatings and ULTIMET™ alloy, and had more carbides, resulting in improved wear resistance [14]. In addition, the chromium in the alloys facilitates the formation of chromium oxide, which resists corrosion. Thus, these alloys, especially STELLITE™ 6 coating may be useful in marine, automotive, aerospace, and oil and gas industries [16,17,53], as well as in components used for bone replacements [5], due to its good wear resistance properties, where a effect of wear is desired.

The addition of 0.3 wt% Ru resulted in an increase in hardness for ULTIMET™, from 386 ± 21 HV_3 to 422 ± 32 HV_3, making a 9.3 % improvement. For STELLITE™ 6, a similar addition of 0.3 wt% Ru increased hardness from 440 ± 25 HV_3 to 543 ± 21 HV_3, a significant 23.4 % increase at 5 N. Furthermore, when 0.6 wt% Ru was added, the hardness of ULTIMET™ increased from 386 ± 21 HV_3 to 466 ± 31 HV_3, representing a 20.7 %. In the case of STELLITE™ 6, the same addition of 0.6 wt% Ru raised hardness from 440 ± 25 HV_3 to 547 ± 39 HV_3 refleting a 24.3 % hardness improvement (Fig. 6).

4.5. Effect of ruthenium on sliding wear of the coatings

Fig. 9 shows higher volume loss and wear rates of bulk and coatings for ULTIMET™ than STELLITE™ at both loads. The volume loss (Fig. 9 a and b) and wear rates (Fig. 9 c and d) for both alloys increased with increased load. This was probably due to frictional heat generated at the contact surfaces, which destroyed the protective surface oxide film that provided some lubrication, reducing wear resistance [8,54]. Once the carbides were lost, then the matrices lost their protection, and also the loose carbides could cause three-body wear.

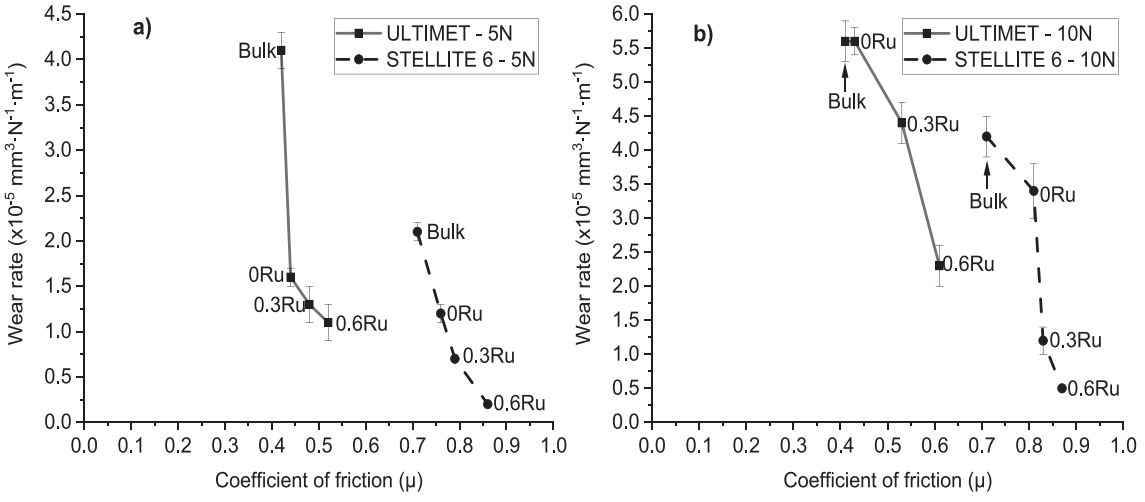


Fig. 14. Relationship between wear rate and coefficient of friction of ULTIMET™ and STELLITE™ 6B bulk alloys, ULTIMET™ and STELLITE™ 6 coatings with ruthenium under sliding wear conditions under: a) 5 N and b) 10 N.

The lower coefficient of friction of bulk ULTIMET™ did not change much when the load was increased, whereas for bulk STELLITE™ 6B there was more fluctuation with the higher load due to much debris collected in the grooves (Figs. 10 and 11) [39], which lowered the friction and wear rate since material was being redeposited on the surface. The lower wear rate of STELLITE™ 6B than ULTIMET™ (Fig. 14) was also due to the chromium-rich carbides that made it harder. Conversely, the higher wear rate of ULTIMET™ was due to its lower coefficients of friction (Fig. 14) and hardness (Fig. 15) than STELLITE™ 6B at both loads. This agreed with previous studies [1,3,7,11,22,23] where hardness was directly proportional to coefficient of friction (Fig. 16) [55,56] and low coefficients of friction gave higher wear rates [1,15] (Fig. 14), and higher hardness gave lower wear rates (Figs. 6, 9 c and d, **14** and **15**) [2,3,57]. Additionally, during the sliding tests, an oxide film (identified by the oxides after wear tests, Table 5) would probably grow and act as a lubricant, decreasing wear rates [9,23].

Table 6 shows the sample-to-ball hypothetical friction patterns I and II, described by Bhushan [2], which were deduced from Fig. 7 and the types of wear experienced by the alloys (Figs. 10–13). Pattern I was interpreted for ULTIMET™ coatings and ULTIMET™ bulk alloy at 5 N and STELLITE™ 6 coatings and STELLITE™ 6B bulk alloy at 10 N, indicating that the 100Cr6 steel ball was harder than the alloys, resulting in ploughing and roughening of the surfaces, whereas ULTIMET™ coatings and ULTIMET™ bulk alloy at 10 N and STELLITE™ 6 coatings and STELLITE™ 6B bulk alloy at 5 N were interpreted to have Pattern II, indicating that the surfaces were smoothened and experienced plastic deformation. Comparing the worn surfaces, ULTIMET™ experienced more mechanical damage than STELLITE™ 6B (Figs. 10 and 11) due to its lower hardness. Despite the high hardness of STELLITE™ 6B, the matrix phase was ploughed out, leaving carbides above the surface (Fig. 11 d), since they were harder and difficult to deform [6]. However, since the same ball type were used in all the wear tests, this shows that there are limitations using the Bhushan approach [2], because the two sets of samples swopped their behaviour at different loads. Alternatively, this shows that the Patterns I and II are closely related, and possibly difficult to distinguish. Mild steel, like all the other samples tested, experienced Pattern III, indicating there was wear debris which was trapped on the wear track, resulting in severe wear damage and higher wear rates.

The sliding wear results of ULTIMET™ and STELLITE™ 6B contradicted those of Liu *et al.* [58] and Ahn and Kwon [59] who found that materials with low coefficients of friction had low wear rates. However, Moore [57] found that the coefficients of friction of materials varied, as did Zang and Battiston [11] for cobalt- and iron-based superalloys and ceramics, and some alloys with low coefficients of friction experienced high wear rates. This could be associated with other factors, such as interface temperature or surface waviness during the tests [60]. Also, two materials (e.g. cobalt- and iron-based superalloys) with the same coefficient of friction exhibited different wear rates [61,62].

The decrease in Si, W and Mo contents, the increase in C, and the gaining of O on the wear tracks of ULTIMET™ and STELLITE™ 6B bulk alloys was a further indication that wear had taken place. The oxygen gained on the wear track was because an oxide film formed, which was facilitated by the high surface temperatures during the sliding wear, and the film was also subsequently broken down, similar to SS41 mild steel [54]. Once this happened, the lubrication effect of the oxide film was reduced and the samples were more prone to wear [8,54]. ULTIMET™ experienced tearing, slip bands and grooves without debris (Fig. 11 a, **12** a and b), while STELLITE™ 6B experienced fewer grooves and more debris.

Thus, all alloys and coatings experienced several wear mechanisms: a mixture of two-body abrasion, which occurred when the harder steel ball slid over the softer and polished surface of the alloys, as well as three-body sliding wear of the cobalt-rich matrix, where debris became the third body when it became trapped between the steel balls and the samples, and acted as an abrasive. The main difference between the sliding wear of these alloys and coatings was that ULTIMET™ alloys and coatings showed deeper groovies and more plastic deformation (Fig. 10 a, **11** a, b, **12** a–c and **13** a–c) than the STELLITE™ 6B bulk alloy and STELLITE™ 6 coatings (Fig. 10 b, **11**c, d, **12** d–f and **13** d–f).

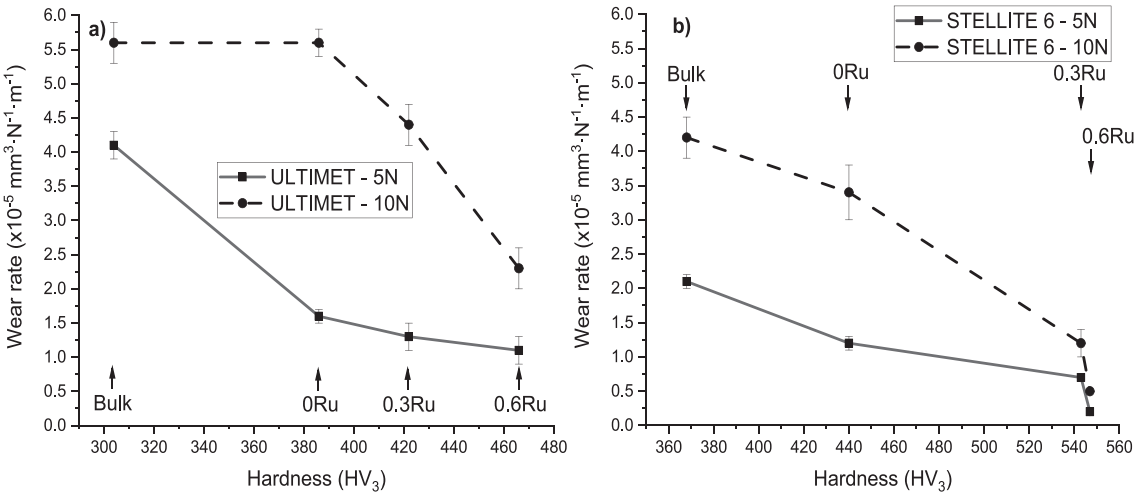


Fig. 15. Relationship between wear rate and hardness (3 kg load) of ULTIMET™ and STELLITE™ 6B bulk alloys, ULTIMET™ and STELLITE™ 6 coatings with ruthenium and mild steel substrate under: a) 5 N and b) 10 N loads.

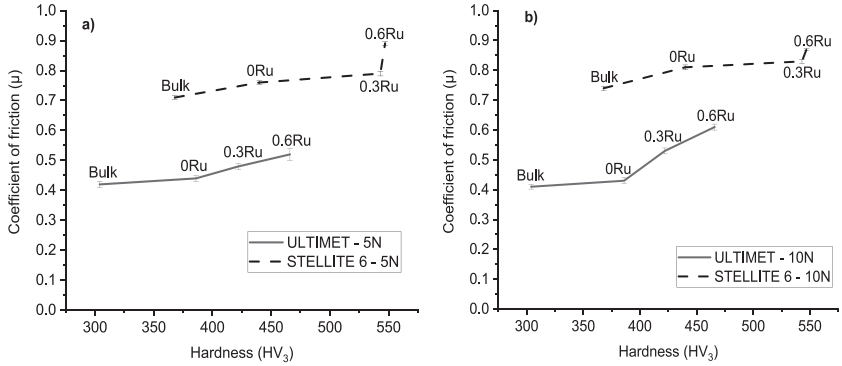


Fig. 16. Relationship between coefficient of friction and hardness of ULTIMET™ and STELLITE™ 6B bulk alloys, ULTIMET™ and STELLITE™ 6 coatings with ruthenium under sliding wear conditions under: a) 5 N and b) 10 N.

Table 6
Hypothetical patterns and coefficients of friction during the sliding of a 100Cr6 steel ball on the ULTIMET™ and STELLITE™ 6B alloys, and ULTIMET™ and STELLITE™ 6 coatings with Ru at 5 and 10 N.

Sample	Pattern and coefficient of friction (μ)			
	5 N		10 N	
	Pattern	μ	Pattern	μ
ULTIMET™ - bulk	I	0.42 ± 0.01	II	0.41 ± 0.04
ULTIMET™ – 0Ru	I	0.52 ± 0.02	II	0.37 ± 0.01
ULTIMET™ – 0.3Ru	I	0.48 ± 0.01	II	0.43 ± 0.01
ULTIMET™ – 0.6Ru	I	0.44 ± 0.01	II	0.43 ± 0.02
STELLITE™ 6B - bulk	II	0.89 ± 0.02	I	0.71 ± 0.04
STELLITE™ 6 – 0Ru	II	0.81 ± 0.02	I	0.79 ± 0.03
STELLITE™ 6 – 0.3Ru	II	0.83 ± 0.01	I	0.78 ± 0.02
STELLITE™ 6 – 0.6Ru	II	0.87 ± 0.02	I	0.81 ± 0.03
Mild steel	III	0.74 ± 0.01	III	0.73 ± 0.02

The addition of 0.3 wt% Ru led to a decrease in wear rate (x10^{-5} $mm^3 \cdot N^{-1} \cdot m^{-1}$)) at 5 N for both ULTIMET™ and for STELLITE™ 6. For ULTIMET™, it reduced from 1.6 ± 0.1 to 1.3 ± 0.2, making an 18.8 % improvement, while for STELLITE™ 6, it decreased from 1.2 ± 0.1 to 0.7 ± 0.0, a remarkable 41.7 % reduction (Fig. 9 c).

When the load was increased to 10 N, wear rates decreased significantly. For ULTIMET™ the wear rate decreased from 5.6 ± 0.5 to 4.4 ± 0.4 (a 21.4 % reduction), and for STELLITE™ 6, from 3.4 ± 0.4 to 1.2 ± 0.00 (a 64.7 % reduction) (Fig. 9 d).

The addition of 0.6 wt% Ru also resulted in decreased wear rates at 5 N. For ULTIMET™, it decreased from 1.6 ± 0.1 to 1.1 ± 0.3 (a 31.3 % reduction), and for STELLITE™ 6, from 1.2 ± 0.1 to 0.2 ± 0.0 (an 83.3 % reduction) (Fig. 9 c). At 10 N, wear rate also decreased from 5.6 ± 0.5 to 2.3 ± 0.3 (a 58.9 % reduction) for ULTIMET™ and from 3.4 ± 0.4 to 0.5 ± 0.0 (a 85.3 % reduction) for STELLITE™ 6 (Fig. 9 d).

Although the 100Cr6 steel ball was used as the counterpart material on the coatings in this study, its surface condition after wear tests or wear rate was not presented. It is important to note that the coatings have a hardness approximately 1.5 times lower than that of the 100Cr6 steel, with the coatings at ~ 550 HV compared to the 100Cr6 steel ~ 800 HV [63,64]. This significant hardness difference, with the 100Cr6 steel ball being 31.3 % harder than the cobalt coatings, raised the expectation that the ball could potentially wear down during sliding. As a result, the coating exhibited propensity for abrasive wear mechanisms when in contact with the steel ball as shown in Figs. 10–13, despite the lack of surface observations of the ball following testing for coatings both with and without ruthenium additive.

Overall, STELLITE™ 6 coatings had lower wear rates and higher coefficients of friction than the ULTIMET™ bulk alloy and coatings, therefore STELLITE™ 6 was the best alloy to resist abrasion at these loads and conditions. The STELLITE™ 6 – 0.6 Ru coating was the hardest (Fig. 6), and exhibited lower wear rates at all loads (Fig. 9), so could be used for coating mild steels operating in wear environments.

5. Conclusions

Sliding wear resistance of mild steel, two cobalt-based bulk alloys, ULTIMET™ and STELLITE™ 6B, and their coatings with minor Ru additions were studied using sliding wear testing at 5 N and 10 N, and the following important coclusions were made:

1. All bulk alloys and coatings comprised of austenite grains with twins and Cr_3C_2 both in the matrix and at grain boundaries. No other carbides such as Cr_7C_3 or $Cr_{23}C_6$ were detected by XRD.

2. ULTIMET^{TM} had slip bands on the surface near the wear track without much debris, while STELLITE^{TM} 6B had some of the matrix ploughed out, leaving carbides on the surface and debris in the grooves during sliding wear.
3. Although ruthenium was not homogeneously distributed within the coatings, the coatings with Ru had better hardness and wear rates than the bulk alloys.
4. The addition of 0.3 wt% Ru improved the hardness of ULTIMET^{TM} by 9.3 % and STELLITE^{TM} 6 by 23.4 %. This resulted in reductions in wear rates, with ULTIMET^{TM} experiencing an 18.8 % decrease and STELLITE^{TM} 6 with a 41.7 % reduction at 5 N. At 10 N, wear rates decreased by 21.4 % for ULTIMET^{TM} and by 64.7 % for STELLITE^{TM} 6. Additionally, addition of 0.6 wt% Ru further increased hardness (by 20.7 % for ULTIMET^{TM} and 24.3 % for STELLITE^{TM} 6) and led to a more wear rate reduction (31.3 % for ULTIMET^{TM} and 83.3 % for STELLITE^{TM} 6) at 5 N. At 10 N, wear rates decreased, by 58.9 % for ULTIMET^{TM} and 85.3 % for STELLITE^{TM} 6.
5. STELLITE^{TM} 6 with 0.6 wt% Ru was the best coating due to its high hardness and low wear rates than all coatings and alloys tested, making it the best candidate for application, such as slurry pump components: casings, sleeves and valves, where a material with a good hardness and wear resistance is required.

Declaration of Competing Interest

The authors declare that they have no known competing financial interests or personal relationships that could have appeared to influence the work reported in this paper.

Data availability

Data will be made available on request.

Acknowledgements

The authors wish to acknowledge the financial support received from the African Materials Science and Engineering Network (A Carnegie-IAS RISE network), as well as Multi Alloys, South Africa for the supply of alloys.

Appendix A. Supplementary data

Supplementary data to this article can be found online at https://doi.org/10.1016/j.engfailanal.2023.107717.

References

[1] P.J. Blau. Friction science and technology: From concepts to applications, 2nd Edn., Taylor and Francis Group, LLC, New York, USA, 2009 https://doi.org/10.1201/9781420054101.
[2] B. Bhushan. Introduction to tribology, 2nd Edn., John Wiley and Sons, New Yok, USA, 2013 https://doi.org/10.1002/9781118403259.
[3] R. Ahmed, H.L. de Villiers Lovelock, S. Davies, Sliding wear of blended cobalt based alloys, Wear 466–467 (203533) (2021) 1–13, https://doi.org/10.1016/j.wear.2020.203533.
[4] X. An, Y. Li, S. Ni, Z. Wang, M. Song, Microstructural and hardness evolutions of a cold-rolled cobalt, Mater. Sci. Eng. A 803 (140712) (2021) 1–9, https://doi.org/10.1016/j.msea.2020.140712.
[5] J. Cawley, J.E.P. Metcalf, A.H. Jones, T.J. Band, D.S. Skupien, A Tribological study of cobalt chromium molybdenum alloys used in metal-on-metal resurfacing hip arthroplasty, Wear 255 (2003) 999–1006, https://doi.org/10.1016/S0043-1648(03)00046-2.
[6] J. Chen, H. Dong, Corrosion and corrosion wear behaviour of plasma carburised stellite 21 Co – Cr alloy, Tribol. Mater. Surfaces Interfaces 3 (1) (2009) 24–30, https://doi.org/10.1179/175158309X419043.
[7] M. Sebastiani, V. Mangione, D. de Felicis, E. Bemporad, F. Carassiti, Wear mechanisms and in-service surface modifications of a stellite 6B Co – Cr Alloy, Wear 290–291 (2012) 10–17, https://doi.org/10.1016/j.wear.2012.05.027.
[8] X. Yang, C. Li, Z. Ye, X. Zhang, M. Zheng, J. Gu, J. Jiang, Effects of tribo-film on wear resistance of additive manufactured cobalt-based alloys during the sliding process, Surf. Coatings Technol. 427 (127784) (2021) 1–14, https://doi.org/10.1016/j.surfcoat.2021.127784.
[9] Z. Zhu, C. Ouyang, Y. Qiao, X. Zhou, Wear Characteristic of Stellite 6 Alloy Hardfacing Layer by Plasma Arc Surfacing Processes, Scanning (2017) 1–7, https://doi.org/10.1155/2017/6097486.
[10] X. Yang, C. Li, M. Zhang, Z. Ye, X. Zhang, M. Zheng, J. Gu, J. Li, S. Li, Dry sliding wear behavior of additively manufactured CoCrWNixAly alloys, Wear 496–497 (2022) 1–21, https://doi.org/10.1016/j.wear.2022.204285, 204285.
[11] K. Zhang, L. Battiston, Friction and wear characterization of some cobalt- and iron-based superalloys in zinc alloy baths, Wear 252 (2002) 332–344, https://doi.org/10.1016/S0043-1648(01)00889-4.
[12] Kennametal Inc., Wrought Wear-Resistant Alloys, https://www.stellite.com/us/en/products/stellite-6b.html, Accessed 20 December 2020.
[13] Haynes International, Ultimet Alloy: Improved Cobalt Chromium Molybdenum Cobalt-Base Alloy, Alloy Digest 42 3: Co–89 1993 10.31399/asm.ad.co0089.
[14] P. Hu, R. Liu, J. Liu, G. McRae, M.X. Yao, R. Collier, Advanced stellite alloys with improved metal-on-metal bearing for hip implants, Mater. Des. 60 (2014) 424–432, https://doi.org/10.1016/j.matdes.2014.04.007.
[15] F.P. Marques, A.C. Bozzi, C. Scandian, A.P. Tschiptschin, Microabrasion of three experimental cobalt-chromium alloys: wear rates and wear mechanisms, Wear 390–391 (2017) 176–183, https://doi.org/10.1016/j.wear.2017.07.023.
[16] K.C. Antony, Wear-resistant cobalt-base alloys, J. Met. 52 (1983), https://doi.org/10.1007/BF03338205.
[17] D. Cooper, F.A. Davis, R.J.K. Wood, Selection of wear-resistant materials for the petrochemical industry, J. Phys. D Appl. Phys. 25 (1992) A195–A204. http://iopscience.iop.org/0022-3727/25/1A/031.
[18] J. Pirso, M. Viljus, K. Juhani, S. Letunovitš, Two-body dry abrasive wear of cermets, Wear 266 (2009) 21–29, https://doi.org/10.1016/j.wear.2008.05.005.

[19] G. Herranz, C. Berges, J. Alfonso, C. García, I. Garrido, Mechanical performance, corrosion and tribological evaluation of a Co – Cr – Mo alloy processed by MIM for biomedical applications, J. Mech. Behav. Biomed. Mater. 105 (2020) 1–11, https://doi.org/10.1016/j.jmbbm.2020.103706.

[20] J. Wen, H. Che, R. Cao, H. Dong, Y. Ye, H. Zhang, J. Brechtl, Y. Gao, P.K. Liaw, Evolution of the mechanical properties of a cobalt-based alloy under thermal shocks, Mater. Des. 188 (108425) (2020) 1–9, https://doi.org/10.1016/j.matdes.2019.108425.

[21] M.X. Yao, J.B.C. Wu, W. Xu, R. Liu, Metallographic study and wear resistance of a high-C wrought Co-based alloy stellite 706K, Mater. Sci. Eng. A 407 (2005) 291–298, https://doi.org/10.1016/j.msea.2005.07.053.

[22] H. Yu, R. Ahmed, H.L. de Villiers Lovelock, S. Davies, Tribo-mechanical evaluations of cobalt-based (Stellite 4) alloys manufactured via HIPing and casting, Proc. World Congr. Eng. 2 (2007) 1385–1390, https://api.semanticscholar.org/CorpusID:1905457ISBN: 9789889867126.

[23] L.E. Falqueto, D.J. Butkus, J.D.B. De Mello, A.C. Bozzi, C. Scandian, Sliding wear of cobalt-based alloys used in rolling seamless tubes, Wear 376–377 (2017) 1739–1746, https://doi.org/10.1016/j.wear.2017.01.009.

[24] T.L. Shing, S. Luyckx, The effect of ruthenium additions on the hardness, toughness and grain size of WC-Co, Int. J. Refract. Met. Hard Mater. Hard Mater. 19 (2001) 41, https://doi.org/10.1016/S0263-4368(00)00048-2.

[25] L. Chipise, P.K. Jain, L.A. Cornish, Influence of Ru on the hardness and fracture toughness of WC-VC-Co alloys, International Journal of Refractory Metals and Hard Materials 77 (2018) 54, https://doi.org/10.1016/j.ijrmhm.2018.07.008.

[26] C. Gao, H. Wang, S. Li, B. Liu, J. Yang, J. Gao, Z. Peng, Z. Zhang, Z. Liu, Enhanced cobalt-based catalysts through alloying ruthenium to cobalt lattice matrix as an Ef Fi cient catalyst for overall water splitting, Electrochim. Acta 327 (2019) 134958, https://doi.org/10.1016/j.electacta.2019.134958.

[27] J.W. van der Merwe, F. Moyo, E.M. Phetla, Corrosion behaviour of ruthenium laser surface alloyed austenitic stainless steel in sulphuric acid and sodium chloride solutions, Mater. Corros. 68 (8) (2017) 815–823, https://doi.org/10.1002/maco.201609343.

[28] O.A. Olaseinde, J.W. van der Merwe, L.A. Cornish, L.H. Chown, P.A. Olubambi, Electrochemical studies of Fe-21Cr-1Ni duplex stainless steels with 0.15 Wt% ruthenium at different temperatures, J. South. African Inst Mining and Metallurgy 112 (2012) 535. http://www.scielo.org.za/scielo.php?script=sci_arttext&pid=S2225-62532012001500007&lng=en&tlng=en.

[29] A.P. Olubambi, J.H. Potgieter, L. Cornish, Corrosion behaviour of superferritic stainless steels cathodically modified with minor additions of ruthenium in sulphuric and hydrochloric acids, Mater. Des. 30 (2009) 1451, https://doi.org/10.1016/j.matdes.2008.08.019.

[30] E.S.M. Sherif, J.H. Potgieter, J.D. Comins, L. Cornish, P.A. Olubambi, C.N. Machio, Effects of minor additions of ruthenium on the passivation of duplex stainless-steel corrosion in concentrated hydrochloric acid solutions, J. Appl. Electrochem. 39 (2009) 1385, https://doi.org/10.1007/s10800-009-9814-5.

[31] S.C.K. Banda, J. van der Merwe, Effect of small additions of ruthenium on pitting corrosion resistance of LDX2101 duplex stainless steel, Corros. Eng. Sci. Technol. 49 (2014) 32–38, https://doi.org/10.1179/1743278213Y.0000000101.

[32] J.H. Potgieter, J. Thomson, F.V. Adams, A.S. Afolabi, Effect of additions of Ru and Pd on the electrochemical behaviour of austenitic stainless steel in organic acids, Int. J. Electrochem. Sci. 9 (2014) 6451–6463, https://doi.org/10.1016/S1452-3981(23)10901-1.

[33] S.I. Hango, Failure of pump systems operating in highly corrosive mine water at otjihase mine, University of the Witwatersrand, Johannesburg, South Africa, 2018 http://wiredspace.wits.ac.za/handle/10539/25666.

[34] S.D. Cramer, B.S. Covino Jr., A.S.M. Handbook, Corrosion : Materials, 13B ASM International, Ohio, United States of America, 2005. ISBN 10: 0871707071.

[35] ASTM International. Standard Test Method for Wear Testing with a Pin-on-Disk Apparatus, West Conshohocken, Pennsylvania USA, 2017, https://doi.org/10.1520/G0099-17.

[36] R. McCaul C. Kaufold Evaluation-of-Coatings-for-Resistance-to-Abrasive-and-Adhesive-Wear-in-Pump-Components, Proceedings of the 9th International Pump Unsers Symposium Turbomachinery Laboratories Department of Mechanical Engineering Texas A&M University USA, 89 95 1992 , doi:10.1520/G0099-17.

[37] T.B. Massalski, Binary Alloy Phase Diagrams, 1, American Society for Metals, Ohio, USA, 1989, ISBN 9780871706218.

[38] G.P. Keeler, Ruthenium synthesis. Physicochemical Properties and Applications, Nova Science Publishers Inc, New York, USA, 2014, 13:9781633216570.

[39] K. Jiang, R. Liu, K. Chen, M. Liang, Microstructure and tribological properties of solution-treated tribaloy alloy, Wear 307 (2013) 22–27, https://doi.org/10.1016/j.wear.2013.08.018.

[40] R. Liu, M.X. Yao, P.C. Patnaik, X. Wu, Effects of heat treatment on mechanical and tribological properties of cobalt-base tribaloy alloys, J. Mater. Eng. Perform. 14 (2005) 634–640, https://doi.org/10.1361/105994905X64567.

[41] S. Al-Qawabah, A. Mostafa, A. Al-Rawajfeh, U. Al-Qawabeha, Effect of heat treatment on the grain size, microhardness and corrosion behavior of the cold-working tool steels AISI D2 and AISI O1, Mater. Tehnol. 54 (2020) 785–790, https://doi.org/10.17222/mit.2020.035.

[42] J. Li, Y. Lu, H. Zhang, L. Xin, Effect of grain size and hardness on fretting wear behavior of inconel 600 alloys, Tribol. Int. 81 (2015) 215–222, https://doi.org/10.17222/mit.2020.035.

[43] M. Sedlaček, B. Podgornik, J. Vižintin, Influence of surface preparation on roughness parameters, Friction and Wear, Wear 266 (2009) 482–487, https://doi.org/10.1016/j.wear.2008.04.017.

[44] H. Yu, H. Deng, W. Huang, X. Wang, The effect of dimple shapes on friction of parallel surfaces, Proc. Inst. Mech. Eng. Part J J. Eng. Tribol. 225 (2011) 693–703, https://doi.org/10.1177/1350650111406045.

[45] B. Wang, M. Zheng, W. Zhang, Analysis and prediction of wear performance of different topography surface, Materials. 13 (5056) (2020) 1–5, https://doi.org/10.3390/ma13225056.

[46] F. Svahn, Å. Kassman-Rudolphi, E. Wallén, The influence of surface roughness on friction and wear of machine element coatings, Wear 254 (2003) 1092–1098, https://doi.org/10.1016/S0043-1648(03)00341-7.

[47] M. Bahshwan, C.W. Myant, T. Reddyhoff, M.S. Pham, The role of microstructure on wear mechanisms and anisotropy of additively manufactured 316L stainless steel in dry sliding, Mater. Des. 196 (2020) 109076, https://doi.org/10.1016/j.matdes.2020.109076.

[48] A. Kešner, R. Chotëborský, M. Linda, The effect of microstructure on abrasive wear of steel, IOP Conf. Ser. Mater. Sci. Eng. 237 (2017), https://doi.org/10.1088/1757-899X/237/1/012040.

[49] B.H. Kim, D.S. Suhr, Characteristics of HVOF-Sprayed Cr3C2 (20 Mas% NiCr) coastings part 2: Effects of heat treatment of the coatings, Mater. Trans. 42 (2001) 870.

[50] P. Zhou, X. Gao, D. Song, Q. Liu, Y. Liu, J. Cheng, Role of Ru on the microstructure and property of novel Co – Ti – V superalloy, J. Mater. Res. (2020) 2737–2745, https://doi.org/10.1557/jmr.2020.251.

[51] P.S. Kevin, A. Tiwari, S. Seman, S.A.B. Mohamed, R. Jayaganthan, Erosion-corrosion protection due to Cr_3C_2-Nicr cermet coating on stainless steel, Coatings 10 (2020) 1–17, https://doi.org/10.3390/coatings10111042.

[52] R. Liu, S.Q. Xi, S. Kapoor, X.J. Wu, Effects of chemical composition on solidification, microstructure and hardness of Co-Cr-W-Ni and Co-Cr-Mo-Ni alloy systems, Int. J. Res. Rev. Appl. Sci. 5 (2010) 110–122. https://www.researchgate.net/publication/49587698.

[53] H. Yu, R. Ahmed, H. de Villiers Lovelock, S. Davies, Influence of manufacturing process and alloying element content on the tribomechanical properties of cobalt-based alloys, J. Tribol. 131 (01160) (2009) 1–12, https://doi.org/10.1115/1.2991122.

[54] K. Hosung, Y. Eui-Sung, K.K. Oh, Self-formation of protective oxide films at dry sliding mild steel surfaces under a medium vacuum, Wear 181–183 (1995) 325–333, https://doi.org/10.1016/0043-1648(95)90039-X.

[55] N.M. Mikhin, K.S. Lyapin, Hardness dependence of the coefficient of friction, Sov. Phys. J. 13 (1972) 317–321, https://doi.org/10.1007/BF00818317.

[56] A. Behera, A.K. Sahoo, Wear behaviour of ni based superalloy: A review, Mater. Today:. Proc. 33 (2020) 5638–5642, https://doi.org/10.1016/j.matpr.2020.04.007.

[57] A.J.W. Moore, W.J. McG, Tegart, relation between friction and hardness, Proc. R. Soc. Lond. Ser. AMathematical and Physical Sciences 212 (1952) 452–458, https://doi.org/10.1098/rspa.1952.0234.

[58] H. Liu, J. Tao, J. Xu, Z. Chen, Q. Gao, Corrosion and tribological behaviors of chromium oxide coatings prepared by the glow-discharge plasma technique, Surf. Coat. Technol. 204 (2009) 28–36, https://doi.org/10.1016/j.surfcoat.2009.06.020.

[59] H. Ahn, O. Kwon, Tribological behaviour of plasma-sprayed chromium oxide coating, Wear 225–229 (1999) 814–824, https://doi.org/10.1016/S0043-1648(98)00390-1.

[60] P.J. Blau, The significance and use of the friction coefficient, Tribol. Int. 34 (2008) 585–591, https://doi.org/10.1016/S0301-679X(01)00050-0.
[61] P.J. Blau, Four great challenges confronting our understanding and modeling of sliding friction, Tribol. Energy Conserv. 34 (2008) 117–128, https://doi.org/10.1016/S0167-8922(98)80067-9.
[62] N.P. Suh, P. Sridharan, Relationship between the coefficient of friction and the wear rate of metals, Wear 34 (1975) 291–299, https://doi.org/10.1016/0043-1648(75)90097-6.
[63] M. Reichelt, B. Cappella, Large scale multi-parameter analysis of wear of self-mated 100Cr6 steel – A study of the validity of archard's law, Tribol. Int. 159 (2021) 106945, https://doi.org/10.1016/j.triboint.2021.106945.
[64] M. Reichelt, B. Cappella, Influence of relative humidity on wear of self-mated 100Cr6 steel, Wear 450–451 (2020) 203239, https://doi.org/10.1016/j.wear.2020.203239.